LAMINAR-TURBULENT TRANSITION AND SHOCK WAVE/BOUNDARY LAYER INTERACTION

Daniel Arnal* and Jean Délery**
* ONERA/DMAE, Toulouse centre, France
** ONERA/DAFE, Meudon centre, France

Summary

Part A: Laminar-turbulent transition. Laminar-turbulent transition strongly affects the wall heat flux of high speed vehicles. The first part of this Lecture is devoted to the description and the modelling of some transition mechanisms. The transition process dominated by the amplification of unstable waves is considered first, with emphasis on the linear stability theory. It is also shown that a major difference between transition in two- and three-dimensional flows lies in the receptivity phase. Then the problem of boundary layer tripping by large roughness elements is briefly addressed.

Part B: Shock wave/boundary layer interaction. Shock wave/boundary layer interactions (SWBLI) in hypersonic flows are characterised by extremely large pressure variations and intense wall heat transfer, especially when the shock is strong enough to separate the boundary layer. The second part of the Lecture focuses on the physical properties of SWBLI induced by a ramp or an impinging-reflecting shock, emphasis being placed on hypersonic interactions. A special attention is paid to thermal effects associated with hypersonic SWBLI. The difficulties raised by SWBLI modelling in high Mach number flows are shortly discussed.

Table of contents

Part A: Laminar-turbulent transition.
1. Introduction
2. The different stages of the "natural" transition process
    2.1 Linear stability theory
    2.2 Non linear phase
    2.3 Receptivity
3. "Natural" transition in 2D flows
    3.1 Multiple modes
    3.2 Receptivity to noise and wind tunnel simulation
    3.3 Some factors affecting transition
4. "Natural" transition in 3D flows
    4.1 Crossflow instability
    4.2 Receptivity to surface roughness
    4.3 Extension of the e^N method
    4.4 Examples of application

Paper presented at the RTO AVT Lecture Series on "Critical Technologies for Hypersonic Vehicle Development", held at the von Kármán Institute, Rhode-St-Genèse, Belgium, 10-14 May, 2004, and published in RTO-EN-AVT-116.

5. Boundary layer tripping criteria
    5.1 General features
    5.2 Some boundary layer tripping criteria
6. Conclusion
7. References

Part B: Shock wave/boundary layer interaction.
1. Introduction
2. Shock wave/boundary layer interaction properties
    2.1 General considerations : The basic interactions
    2.2 The compression ramp flow
    2.3 The impinging-reflecting oblique shock
    2.4 Supersonic separation and the free interaction theory
    2.5 Features of the wall pressure distribution
    2.6 Thermal effects in hypersonic interactions
        2.6.1 Wall temperature effects on the interaction properties
        2.6.2 Heat transfer in hypersonic interaction
    2.7 Real gas effects on shock wave/boundary layer interaction
    2.8 Entropy layer effect
    2.9 Transitional shock wave/boundary layer interactions
3. Problems raised by interaction prediction
    3.1 Code numerical accuracy
    3.2 The physical models
4. Conclusion
5. References

PART A. LAMINAR-TURBULENT TRANSITION

1. Introduction

For many years, the instability of laminar boundary layer flows and the transition to turbulence have maintained a constant interest in fluid mechanics problems. This interest results from the fact that transition controls important aerodynamic quantities such as drag or heat transfer. For example, the heating rates generated by a turbulent boundary may be several times higher than those for a laminar boundary layer, so that the prediction of transition location is of great importance for hypersonic re-entry spacecraft, because the thickness of the thermal protection system (TPS) is strongly dependent upon the altitude where transition occurs.

There are many aspects of the transition problems. Due to space limitation, only some of them will be discussed in this paper. In paragraphs 2 to 4, emphasis will be placed on "natural" transition, i.e. on transition process dominated by the development of unstable waves. Paragraph 2 gives a general review of the different stages of the transition process and of their modelling. Specific problems linked to transition in two-dimensional flows (multiple modes, wind tunnel simulation, factors affecting transition) are reviewed in paragraph 3, whilst paragraph 4 concentrates on the specific aspects of transition in three-dimensional flows. It will be shown that the so-called crossflow instability, which is a peculiar feature of these flows, exhibit properties which are completely different from those of two-dimensional (streamwise) instability. Paragraph 5 addresses another laminar-turbulent transition mechanism in which "natural" instabilities do not play the major role: this is the problem of boundary layer tripping by isolated roughness elements. In this case, there is no general theory available today, so that the use of purely empirical criteria becomes necessary for application purposes. A review of the most popular criteria is given in this paragraph.

2. The different stages of the "natural" transition process

To describe the laminar-turbulent transition process in two-dimensional (2D) or three-dimensional (3D) flows, it is usual to distinguish three successive steps. The first step, which takes place close to the leading edge, is called *receptivity*. Receptivity describes the means by which forced disturbances such as free-stream noise, free-stream turbulence, vibrations, small roughness elements… enter the laminar boundary layer and excite its eigenmodes. In the second phase, these eigenmodes take the form of periodic waves, the energy of which is convected in the streamwise direction. Some of them are amplified and will be responsible for transition. Their evolution is fairly well described by the *linear stability* theory. When the wave amplitude becomes finite, *non linear interactions* occur and lead rapidly to turbulence.

The general features of these three steps are described below, by beginning with the linear phase which is rather well known for many years. The investigations on the non linear phase and on receptivity are much more recent. The application of these results to 2D and 3D flows is the subject of paragraphs 2 and 3.

2.1 Linear stability theory

The principle of this theory is to introduce small sinusoidal disturbances into the Navier-Stokes equations in order to compute the range of unstable frequencies (see details in [1]). Any fluctuating quantity r'(velocity, pressure, density or temperature) is expressed by:

$$r' = \hat{r}(y)\exp\left[i(\alpha x + \beta z - \omega t)\right]$$

$\hat{r}$ is an amplitude function and y is normal to the surface. In the particular case of a swept wing, x is often measured along the wing surface in the direction normal to the leading edge, z is the spanwise direction. In general, α, β and ω are complex numbers. α and β represent the wave number components in the x and z directions; ω represents the wave frequency.

The fluctuating quantities are very small, so that the quadratic terms of the disturbances are neglected in the Navier-Stokes equations. It is also assumed that the mean flow quantities do not vary significantly over a wavelength of the disturbances; therefore U and W (mean flow components in the x and z directions) as well as the mean temperature T are functions of y alone, and the vertical velocity V is equal to zero. The implication of this parallel flow assumption is that the stability of the flow at a particular location (x,z) is determined by the local conditions at that location independently of all others.

This leads to a system of homogeneous, ordinary differential equations for the amplitude functions. For two-dimensional, low speed flows, these equations reduce to the well-known Orr-Sommerfeld equation, the solutions of which represent the classical Tollmien-Schlichting waves. Due to the homogeneous boundary conditions, the problem is an eigenvalue one: for a given mean flow field, non trivial solutions exist for certain combinations of the parameters α, β, ω and R, where R is the Reynolds number. This constitutes the dispersion relation.
In this paper, the discussion will be restricted to the spatial theory, i.e. to the transition mechanisms governed by a convective instability. In this case, ω is real and α is complex. For the sake of simplicity, it will be assumed that β is also real. Therefore r' is expressed by:

$$r' = \hat{r}(y)\exp(-\alpha_i x)\exp\left[i(\alpha_r x + \beta z - \omega t)\right]$$

The spatial growth rate $-\alpha_i$ is the opposite of the imaginary part of α, α_r being the real part. The wave number vector $\vec{k} = (\alpha_r, \beta)$ makes an angle ψ with respect to the x direction. When the mean flow is specified, the eigenvalues α_r and α_i are computed for imposed values of β, ω and R. In the (R, ω) diagram, a neutral curve ($-\alpha_i = 0$) separates the stable region where the disturbances are damped ($-\alpha_i < 0$) from the unstable region ($-\alpha_i > 0$) where the disturbances are amplified.

The linear PSE (Parabolized Stability Equations) approach provides an improvement to the classical, local theory described above [2]. The mean flow field and the amplitude functions now depend on both x and y, and α depends on x. With the assumption that the x-dependence is slow, the numerical problem consists in solving a set of (nearly) parabolic equations in x, with initial disturbance profiles specified at some starting point x_0. The PSE make it possible to take into account the flow history (non local approach), the nonparallel effects as well as the wall curvature. When local and non local results are compared, it is observed that the growth rates are quite similar for two-dimensional waves (i.e $\psi = 0°$). This conclusion, however, is no longer valid for oblique waves (i.e $\psi \neq 0°$); in this case, the mean flow non-parallelism exerts a destabilising effect, which increases with increasing Mach numbers [3].

To predict transition, the most popular method is the e^N criterion. The so-called N factor is the total growth rate of the most unstable disturbances. It is computed by integrating $-\alpha_i$ in the streamwise direction. It is assumed that transition occurs for some specified value of N; for instance, the N factor at transition lies in the range from 8 to 10 on 2D airfoils in low turbulence wind tunnels. A comprehensive discussion on the application of the e^N method can be found in [4]. Some examples of high speed flow results are provided in the next paragraphs.

2.2 Non linear phase

The main interest of the linear PSE is to provide initial conditions for the non linear PSE which simulate the non linear wave interactions [2]. The disturbances are now expressed as a double series of (*n, m*) modes of the form:

$$r' = \sum_{n=-\infty}^{n=+\infty} \sum_{m=-\infty}^{m=+\infty} \hat{r}_{nm}(x,y) \exp\left[i\left(\int \alpha_{nm}(\xi) d\xi + m\beta z - n\omega t\right)\right]$$

α_{nm} is complex, β and ω are real numbers. The integers n and m characterise the frequency and the spanwise wave number, respectively. When these disturbances are introduced into the Navier-Stokes equations, a system of coupled partial differential equations is obtained; it is solved by a marching procedure, as it was already the case for the linear PSE. Any non linear PSE computation requires i) to choose the "most interesting" interaction scenario between particular modes which are referred to as major modes ii) to impose initial amplitudes A_0 for the major modes. For 2D flows, non linear computations end with a sudden increase of the major modes and of their harmonics; this simulates the breakdown to turbulence. For 3D flows, the non linear interactions result in a saturation of the amplitude of all the modes, without any indication of breakdown. It is then necessary to use a secondary instability theory to predict transition. Due to space limitation, a detailed description of the non linear mechanisms will not be given in this paper.

2.3 Receptivity

As explained before, receptivity is the word which is used to describe the link between the excitation sources and the initial amplitude A_0 of the boundary layer eigenmodes. Two important results are: i) A_0 increases when the amplitude of the excitation increases and ii) a perturbation of frequency f excites waves having the same frequency.

There are important consequences of the second result. For instance, if there is no excitation of frequency f, then there is no chance to observe waves of frequency f travelling in the boundary layer, even if these waves are unstable according to the linear stability theory. As it will be shown in the following two paragraphs, the receptivity process is completely different for 2D and for 3D flows.

As a first approximation, it can be assumed that transition occurs for a more or less "universal" value A_t of the most amplified wave amplitude. A_t and the initial amplitude A_0 of the wave are linked together through the N factor at transition: $A_t = A_0 \exp(N)$. This shows that increasing A_0 (i.e increasing the amplitude of the excitation) will reduce N at transition. In other words, N is a measure of the quality of the disturbance environment.

3. "Natural" transition in 2D flows

3.1 Multiple modes

An important aspect of instability for compressible flows is the effect of the wave number direction ψ on the amplification rates. Up to Mach numbers of the order of 0.7 to 0.8, the maximum value of $-\alpha_i$ (for a given Reynolds number) usually corresponds to $\psi \approx 0°$. At transonic Mach numbers, the largest growth rates are obtained for non zero values of ψ (oblique waves). Typically, the most unstable direction is around 40 or 50° for Me (free-stream Mach number) close to 1.

For flat plates up to $Me = 2.2$ on adiabatic wall, the unstable region in the (R, ω) diagram is contained into a single curve. At higher Mach numbers, the waves become supersonic relative to the mean flow close to the wall; this results in the generation of higher modes first

discovered by Mack for boundary layer flows [1]. Two stability diagrams are presented in figure 1 for *Me* = 4.5 and two values of ψ: 0 and 60º [5]. For ψ = 0º, two unstable loops are visible. The unstable region associated with low values of ω is the equivalent of the unique unstable region observed at low Mach number; it is referred to as the first mode. The second loop, at higher frequencies, is the second mode resulting from the existence of the supersonic waves as explained before. There is an infinity of other (stable or unstable) modes associated with higher and higher frequencies. The results for ψ = 60º on the right hand side of Figure 1 show that changing the wave orientation stabilises the second mode, but increases the instability of the first one. This is a general rule: systematic computations demonstrated that the most unstable first mode disturbances are oblique, whilst the most amplified second mode waves are two-dimensional.

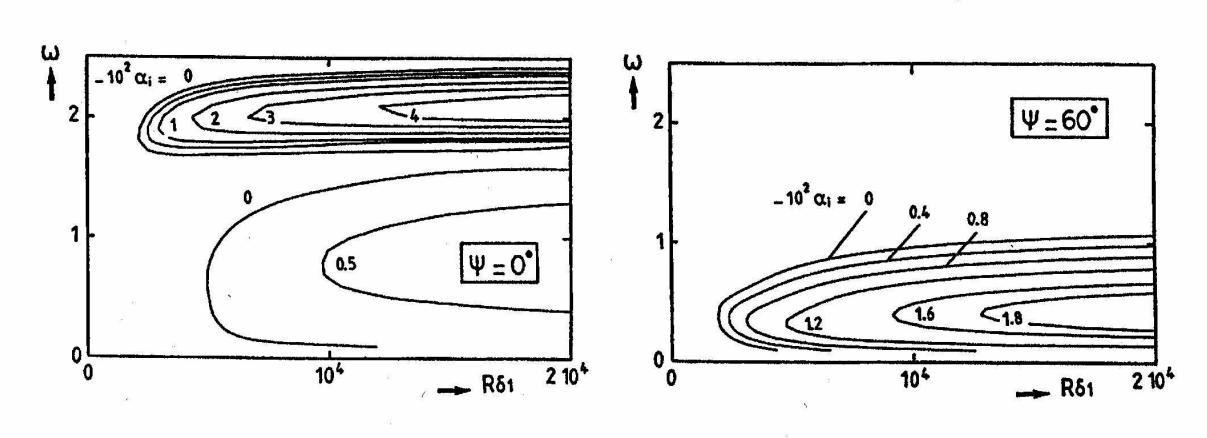

Figure 1. Effect of wave orientation on the growth rate (Me = 4.5)
$R\delta 1$ is the displacement thickness Reynolds number, α_i is made dimensionless with $\delta 1$, ω is made dimensionless with $\delta 1$ and the free stream velocity Ue

3.2 Receptivity to noise and wind tunnel simulation

In supersonic and hypersonic wind tunnels, the main factor affecting transition on 2D models is the noise, the origin of which lies in the pressure disturbances radiated by the turbulent boundary layers developing along the nozzle walls. This leads to low transition Reynolds numbers, i.e. to small values of the *N* factor at transition. Empirical relationships have been proposed, which illustrate the fact that the transition Reynolds numbers (and the corresponding *N* factors) decrease with increasing free-stream pressure fluctuations in the nozzle, see review in [5]. Typical values of the transition *N* factor are in the range between 1 and 5 for classical high speed ground facilities.

When the unit Reynolds number increases (for a fixed value of the Mach number), the range of unstable waves shifts to higher frequencies. In the free stream, the energy of the corresponding pressure fluctuations decreases, so that the transition Reynolds number increases; this is one of the explanations of the unit Reynolds number effect.

Since the radiated noise is inherent in the presence of walls around the model, there is little doubt concerning the incapacity of conventional ground facilities to properly simulate free flight conditions. In order to reduce this noise level, it is necessary to delay transition on the nozzle walls, because a laminar boundary layer is less noisy than a turbulent one. This was done in the “quiet tunnel” built at NASA Langley with a free-stream Mach number equal to 3.5, see description in [6]. Notable features are the use of boundary layer bleed slots upstream

of the throat, a careful polishing and a careful design of the nozzle walls contour in order to minimise the development of Görtler vortices. With a laminar boundary layer on the nozzle walls, the measured pressure fluctuations can be one or two orders of magnitude below those measured in conventional facilities.

Several transition experiments were carried out in the "quiet tunnel". On simple 2D bodies (flat plates, cones at zero angle of attack), large transition Reynolds numbers were measured. They correspond to N factors around 10, i.e. several times the value found in conventional (noisy) facilities [7]. The problem is to know what is the value of N in real flight conditions.

Figure 2 shows flight transition results collected for sharp cones by Beckwith [8]. The transition Reynolds numbers Rx_T based on the streamwise distance are plotted as function of the free-stream Mach number. The figure also contains a correlation for wind tunnel transition data, which lies much below the flight results. Malik [9] calculated the theoretical values of Rx_T corresponding to $N = 10$ for a 5° half angle cone and for Mach numbers up to 7. He made two series of computations, one by assuming that the wall was adiabatic (curve *a*), and the other by assuming that the wall was cold according to a certain empirical law. In spite of the large scatter in the flight data, it can be seen that the computations with a cold wall (curve *b*) are in qualitative agreement with the flight results. Quiet tunnels are currently under development at Purdue University [10] and at ONERA [11]. Design and operational details of NASA Langley quiet supersonic wind tunnels are described in [12].

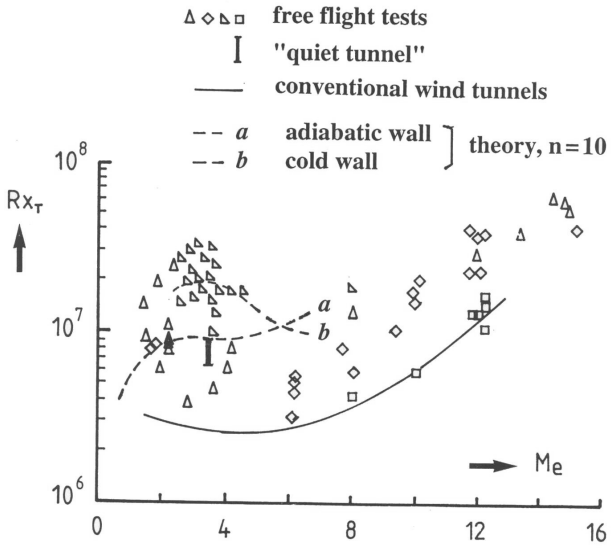

Figure 2. Comparison between measured and predicted Reynolds numbers on sharp cones

The conclusion is that the e^N method with $N \approx 10$ can be applied to predict transition in high speed 2D flows developing on smooth walls if the background disturbance level is low enough (free flight, "quiet" facilities).

3.3 Some factors affecting transition

When **wall cooling** is applied, the stability properties change dramatically. Cooling a wall strongly stabilises first mode disturbances and has less effect on second mode disturbances. At low Mach numbers, very large values of the transition Reynolds number Rx_T can be achieved with a moderate cooling. At high Mach numbers, the ratio Rx_T / Rx_{T0} (where Rx_{T0} is

the transition Reynolds number in adiabatic conditions) becomes nearly independent of the wall temperature. These trends have been observed in wind tunnels and in flight conditions; they have been confirmed by linear stability computations [5].

In hypersonic flows, a small **nose bluntness** of a cone at zero angle of attack or a small **leading edge bluntness** of a flat plate strongly affects the transition location because it reduces the local Reynolds number and creates a negative pressure gradient which stabilises the flow. As a result, transition is delayed. For instance, Malik et al [13] performed a linear stability analysis for the experimental conditions studied by Stetson et al [14] at a Mach number equal to 8. The model was a cone which could be equipped with interchangeable spherically blunted noses. By using the e^N method, Malik et al found that the predicted transition Reynolds number increased due to small nose bluntness, in qualitative agreement with experimental results. They also demonstrated that nose bluntness could explain the unit Reynolds number effect observed in aeroballistic range experiments.

In the framework of a TRP (Technological Research Programme) initiated by ESA (European Space Agency), the effect of nose bluntness was studied in the case of a cone placed at zero angle of attack in a wind tunnel at Mach 7 (unit Reynolds number = 25 10^6 m^{-1}, length of the model = 20 cm). Three values of the cone nose radius *Rn* were considered: *Rn* = 0 (sharp cone), 0.2 mm and 0.5 mm. The experimental results indicated that the onset of transition moved downstream with increasing *Rn*, in agreement with previous investigations [15,16].

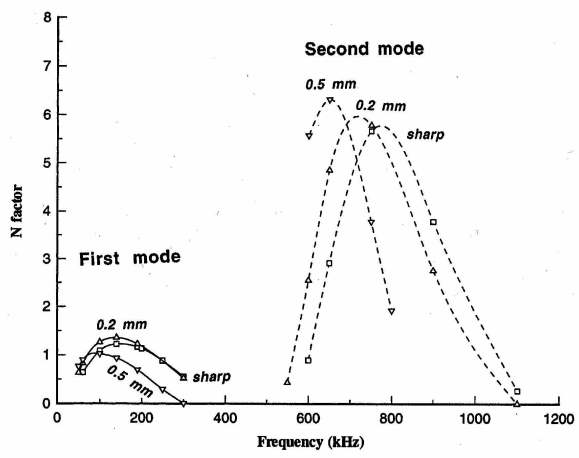

Figure 3. Integrated growth rates at transition for blunt cones

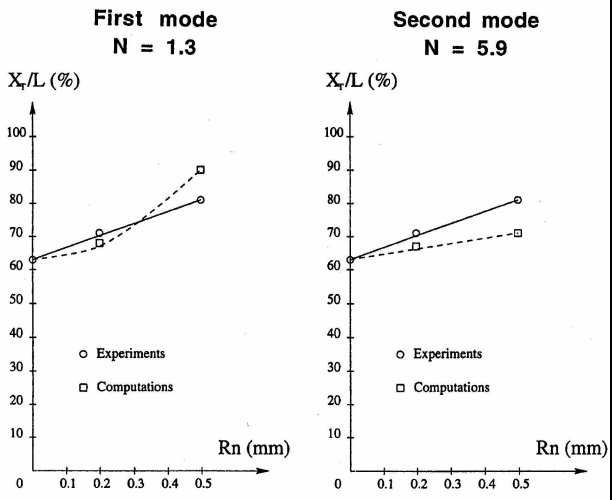

Figure 4. Blunt cone: measured and computed transition locations

For the numerical analysis of these experiments, the mean flow field was computed by solving the steady Navier-Stokes equations. Then linear computations were performed by using the CASTET code developed at ONERA. The integrated growth rates at transition are plotted in Figure 3 as a function of the disturbance frequency. As expected, the frequency ranges for first and second mode disturbances are clearly separated. First mode waves are around 150 kHz, while second mode waves are around 700 kHz. We now assume that transition occurs when the *N* factor for first and second mode waves reaches a fixed value. This value is taken from the sharp cone results (*N* = 1.3 for the first mode, *N* = 5.9 for the second mode). The theoretical and measured transition locations are plotted in Figure 4 as a

function of *Rn*, by considering separately first and second mode disturbances. The agreement is quite good for *Rn* = 0.2 mm. For *Rn* = 0.5 mm, the transition abscissa is overestimated when first mode waves are considered, while it is underestimated when second mode waves are considered. As the differences with experimental data are nearly the same, it is very difficult to decide which mode is responsible for transition. However it is not clear that free-stream disturbances in a frequency range around 700 kHz exist in the wind tunnel. Therefore first mode disturbances only are likely to be excited by the available free stream environment.

When the nose or leading edge bluntness becomes large, the downstream movement of transition is no longer observed; on the contrary transition begins to move upstream. This phenomenon is not fully understood today.

Two explanations for the **unit Reynolds number effect** observed in many wind tunnel measurements have been pointed out before: mainly the change in the unstable frequency range (paragraph 3.2) and, in some cases, the nose or leading edge bluntness effect. As a result, the transition Reynolds number on a given model at a given Mach number increases with increasing unit Reynolds number.

At hypersonic speeds, the gas often cannot be modelled as perfect because the molecular species begin to dissociate due to aerodynamic heating. A few papers have been devoted to the analysis of **real gas effects** on stability properties. For instance, Figure 5 shows the variation of the growth rate as a function of a dimensionless frequency *F* for a flat plate flow at Mach 10 ($Rx = 4\ 10^6$, *Te* = 350 K, adiabatic wall) [17,18]. The computations have been performed for ideal gas, chemical equilibrium and non equilibrium. In the latter two cases, a third unstable mode appears, and instability is enhanced for the second mode.

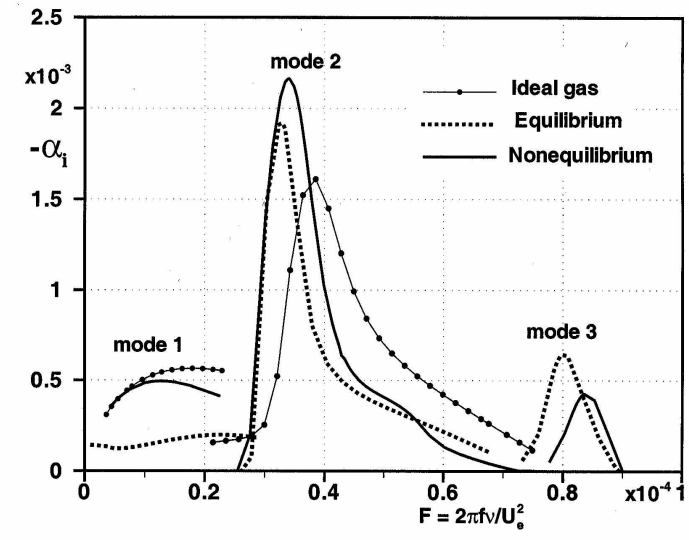

Figure 5. Real gas effects on stability properties

4. "Natural" transition in 3D flows

4.1 Crossflow instability

The mean velocity profile of a boundary layer developing on a three-dimensional body can be decomposed into a streamwise mean velocity profile u (in the direction of the external streamline) and a crossflow velocity profile w (in the direction normal to this streamline). Figure 6 shows a schematic view of the boundary layer development on a swept wing, with a negative pressure gradient in the leading edge region and a positive pressure gradient further downstream.

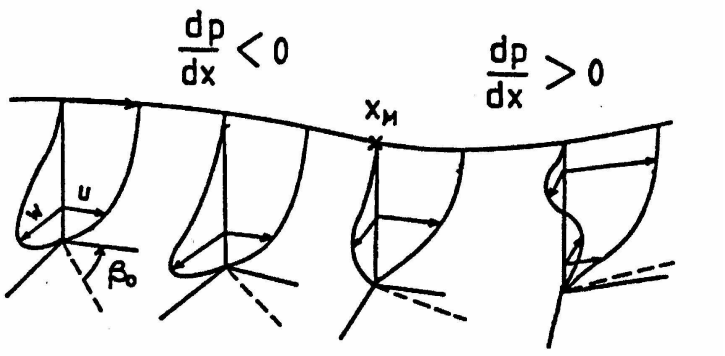

Figure 6. Laminar boundary layer development on a swept wing. X_M is the location of the inviscid streamline inflection point, β_0 is the angle between the wall and potential streamlines

As the streamwise mean velocity profiles look like classical two-dimensional velocity profiles, their instability properties are qualitatively similar to those of two-dimensional flows; in particular first and second mode disturbances are likely to exist at large Mach numbers. This corresponds to the **streamwise instability**. On the other side, an inflection point is always present in the crossflow mean velocity profile. As a consequence a powerful inflectional instability is expected to occur in regions where w develops rapidly. This phenomenon is called **crossflow instability**. It is observed, for instance, in the vicinity of the leading edge of a swept wing, a region where the crossflow mean velocity profile w develops rapidly due to the strong negative pressure gradient. The wave number direction ψ_M of the crossflow waves (relative to the external streamline) is never exactly equal to 90°. It lies in a narrow range close to the crossflow direction, say between 80 and 89°.

Let us notice that the unstable frequency range is usually wider for crossflow instability than for streamwise instability. In particular, linear stability theory shows that crossflow instability can amplify zero frequency disturbances. This leads to the formation of stationary vortices, the axes of which are close to the streamwise direction. These vortices can be visualised as streaks on the surface, as it can be seen on the infrared picture presented in the left hand part of Figure 7. The picture corresponds to supersonic experiments performed at Mach 3 on a swept wing in the R1Ch wind tunnel at ONERA [19,20]. The right hand part shows the spanwise variation of the mean wall temperature measured in the area of the ellipse drawn in the left hand part. From this curve a spanwise wavelength close to 1.5 mm can be deduced, in very good agreement with linear stability theory.

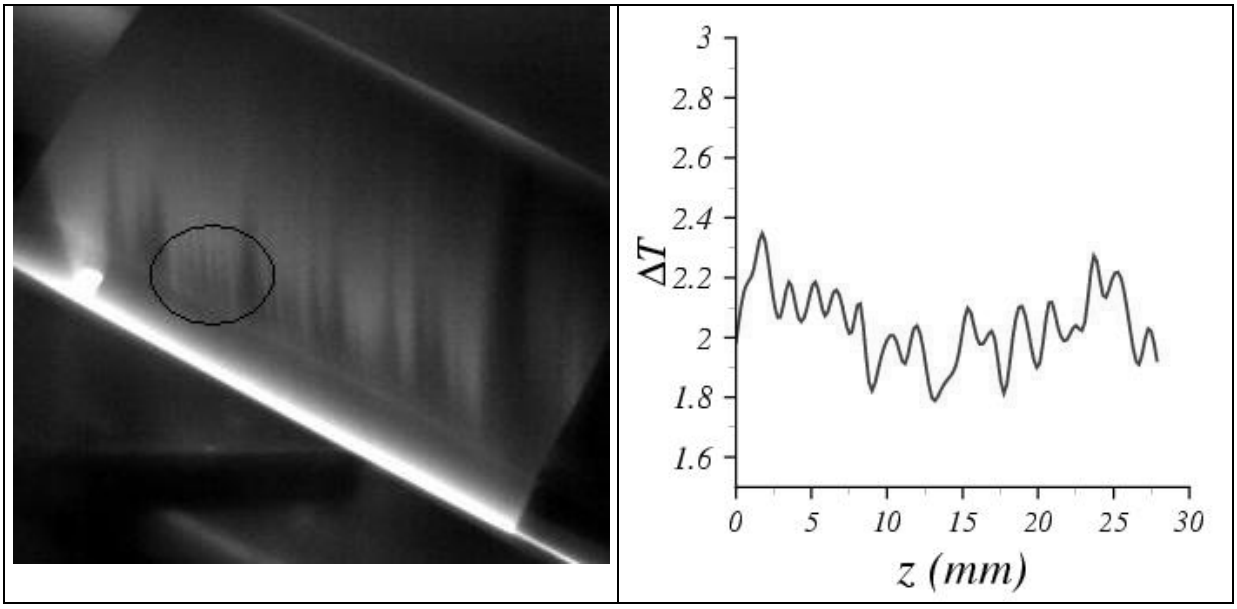

Figure 7. Stationary vortices on a swept wing at supersonic Mach number (Me = 3)

4.2 Receptivity to surface roughness

For 2D flows, it has been shown previously that the unstable waves are mainly excited by the free-stream noise. This is no longer true for 3D flows when transition is governed by a "pure" crossflow instability. In this case, the stationary vortices mentioned before play the major role in the transition process by creating a steady inflection point in the streamwise mean velocity profile. It follows that noise has only a small effect on the receptivity mechanisms and on transition (as observed by King [21]).

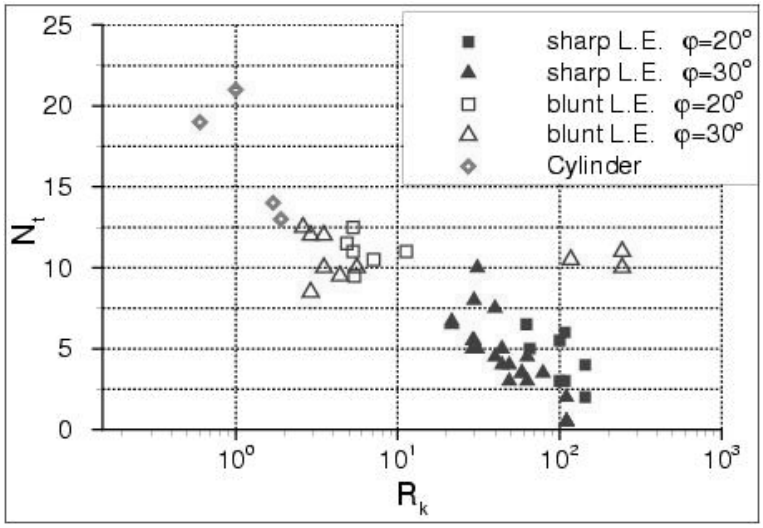

Figure 8. Transition N factor for crossflow instability as a function of a roughness Reynolds number

According to the statement that waves of frequency *f* are generated by excitations of the same frequency, one has to look at stationary excitations to explain the origin of the vortices. For low speed flows, Radetsky et al [22] demonstrated that micron-sized roughness elements,

i.e. surface polishing, is the main factor influencing the generation of the stationary vortices and hence the transition location. This statement seems to remain true for high speed flows, at least at supersonic Mach numbers. This was demonstrated by several series of experiments carried out at Mach 3 in the R1Ch wind tunnel at ONERA on a swept cylinder, on a swept wing equipped with a sharp leading edge and on the same swept wing equipped with a blunt leading edge (the results in Figure 7 were obtained on the swept wing with blunt leading edge) [19,20]. As shown in Figure 8, there is a clear correlation between the transition N factor computed for stationary vortices and the Reynolds number $R_k = U_k\, k/\nu_k$. k is a measure of the surface polishing (between 1 and 10 μm), U_k and ν_k are the mean velocity and the kinematic viscosity at $y = k$. It can be expected that a similar correlation exists for hypersonic Mach numbers. This result is very important, because it implies that significant 3D transition studies could be performed even in noisy wind tunnels.

4.3 Extension of the e^N method

For the purpose of transition prediction, the e^N method can also be applied for 3D flows. For large Mach number, one has to compute three different N factors:

- one corresponding to "low" frequency first mode disturbances generated by the u velocity profile;
- one corresponding to the "high" frequency second mode disturbances generated by the same profile;
- one corresponding to the "very low" crossflow disturbances generated by the w profile.

In practical problems, it is not always easy to make a clear distinction between first mode and crossflow disturbances, because both of them are oblique waves with wave number directions which can be close together. Another important remark concerns the value of the transition N factor. As the three types of disturbances listed above cover very different frequency ranges and because the receptivity process is very different for streamwise and for crossflow disturbances, there is little doubt that different transition N factors need to be imposed for each type of unstable waves. This point is illustrated below.

4.4 Examples of application

Up to now there are only a few results dealing with the application of the e^N method for 3D supersonic and hypersonic flows. Most of the geometries which have been studied so far are cones at angle of attack and swept (or delta) wings with blunt leading edges.

Cones at angle of attack. Transition on a cone at incidence usually occurs earlier on the leeward line of symmetry than on the windward line. As there is no azimuthal mean velocity component along these lines, their stability properties are those of 2D flows (at least in the framework of the classical linear stability theory). Away from the windward and leeward rays, crossflow instability can dominate and cause transition.

In the framework of the ESA TRP mentioned before, experiments and computations have been performed for a cone at Mach 7 and 2 degree angle of attack [23]. Figure 9 shows the integrated growth rates of first and second mode disturbances at the measured transition location on the leeward ray (meridian angle $\phi = 180°$) and on the windward ray (meridian angle $\phi = 0°$). Results at zero angle of attack are given for comparison. The most striking feature is that the second mode calculated frequency range is extremely high, about 1000 kHz. As for the bluntness problem, its contribution to transition seems unrealistic: there are certainly no free-stream disturbances in this frequency range. This is confirmed by the fact that applying the e^N method to second mode disturbances gives a transition location on the

leeward ray downstream of the transition location on the windward ray, which disagrees with the experimental data (first mode disturbances, on the contrary, exhibit the correct trend). Therefore second mode disturbances will not be taken into account in the analysis.

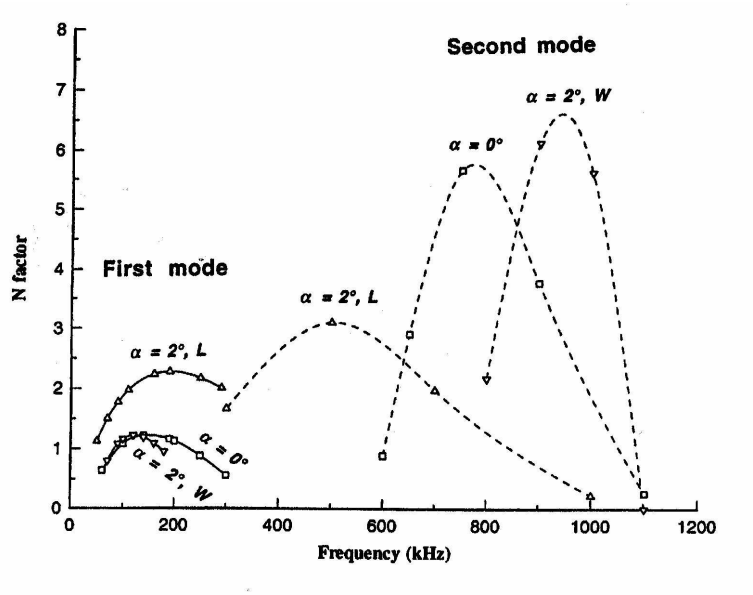

Figure 9. N factors at transition on a cone at angle of attack (L: leeward, W: windward)

Without incidence, the first mode wavenumber vector directions are around ± 65°. With incidence, the wavenumber vector turns to around - 88° along the ray corresponding to ϕ = 90°. Hence, the first mode becomes a "first/crossflow" mode, a nice candidate for transition correlation in the area around ϕ = 90°. On the leeward and windward rays, both *w* and crossflow instability disappear. The conclusion is that there is no single mode which is responsible for transition over the entire cone. As shown in Figure 10, transition is associated with the first mode close to the vertical plane of symmetry, and with "first/crossflow" mode around ϕ = 90°. The numerical transition line is quite comparable to the experimental line. It should be stressed that these two modes are associated with quite different values of the *N* factor, about 1 for the first mode and about 5 for the "first/crossflow" mode. Details of these computations can be found in [15,16].

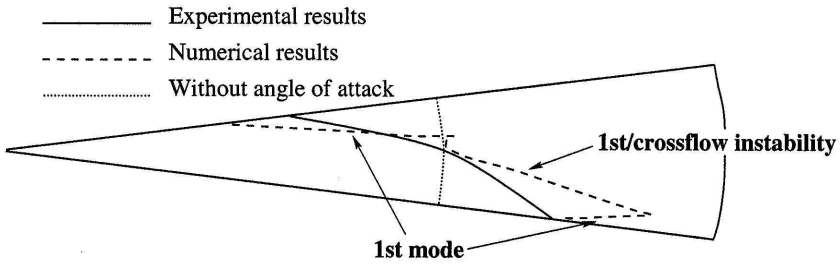

Figure 10. Measured and computed transition lines on a cone at incidence

Linear stability computations for cones at angle of attack have also been performed by Malik and Balakumar [24] and by Hanifi [25] at lower Mach numbers. Hanifi used a PSE approach and observed that the non local effects on the first mode disturbances were larger on the windward ray than on the leeward ray.

Swept models. Transition on a swept wing leading edge model at Mach 3.5 was investigated by Cattafesta et al [26]. Numerical results obtained with the e^N method were compared to experimental transition location measured in the NASA Langley "quiet tunnel". It was found that traveling disturbances with $N \approx 13$ provided a good correlation with experiments over a range of unit Reynolds numbers and angles of attack.

The transition process on a delta wing was investigated at Imperial College gun tunnel within ESA TRP [23]. A large number of parameters (angle of attack, angle of sweep, unit Reynolds number, leading edge bluntness) was investigated at a Mach number equal to 8.8. Linear, local stability computations have then been performed for a few experimental configurations [15,16]. With sharp leading edges, the boundary layer development was nearly 2D and measured transition locations were correlated with N factors between 1 and 2. As soon as the leading edge radius was increased, the boundary layer flow became highly 3D, and transition was provoked by crossflow instability at significantly larger values of the N factor. This confirms that N factors at transition are likely to be very different depending on the type of dominant instability.

5. Boundary layer tripping criteria

5.1 General features

In many practical applications, for instance on re-entry vehicles, transition does not occur "naturally" in the sense that it is triggered by roughness elements. Therefore many empirical boundary layer tripping criteria have been established. In Europe, after transition work related to the HERMES project, the ESA TRP on transition gave the opportunity to conduct roughness induced transition experiments in a (noisy) wind tunnel and to review existing criteria [27]. In case of the US space shuttle, the use of a tiled TPS over the lower surface is responsible for a quite distributed roughness which triggers transition in the re-entry phase. Flight data and wind tunnel results were used to validate existing criteria, to improve them or to develop new criteria.

It is now recognised today that 2D roughness elements (gaps, steps of "infinite" span) are less efficient for boundary layer tripping than 3D isolated or distributed roughness elements like spheres, cylinders or cones. In the later case, a very complex 3D flow develops around the obstacle. This leads to the formation of streamwise vortices which breaks down into turbulence some distance downstream of the roughness element; this point corresponds to the apex of a turbulent wedge which spreads more or less rapidly downstream. It is important to note that boundary layer tripping on the space shuttle is triggered by surface irregularities resulting from the corners of misaligned tiles, which can be considered as 3D, randomly spaced roughness elements.

A comprehensive review of all transition criteria available in the literature for 3D roughness elements (isolated or distributed) is out of the scope of this paper. Only the most popular of them are briefly described below. They provide the value of the roughness height k which provokes transition. Sometimes distinction is made between the "critical" roughness height and the effective roughness height k_{eff}. The critical roughness is the roughness which begins to move the transition point upstream of its natural position. The effective roughness is

the roughness for which the apex of the turbulence wedge reaches its more upstream position. For Me = 0, this position is the roughness location. When the free-stream Mach number increases, a non-zero distance L exists between the roughness element and the apex of the wedge. For a fixed value of Me, L remains constant for $k > k_{eff}$, see discussion in [5].

5.2 Some boundary layer tripping criteria

The well-known **van Driest and Blumer** [28] criterion, developed for isolated spherical roughness elements placed over cones, is written in its original form:

$$Rk_{eff} = 33.4\left[1+\frac{\gamma-1}{2}Me^2 - 0.81\frac{Taw - Tw}{Te}\right]Rx_k^{0.25}$$

where Rk_{eff} (respectively Rx_k) is a Reynolds number calculated with the free-stream conditions and with the effective roughness height (respectively with the roughness location x_k). Me, Te, Tw and Taw are the free stream Mach number, the free stream static temperature, the wall temperature and the adiabatic wall temperature. A critical study of this criterion can be found in [29]. More recently, NASA modified the original expression with application to Shuttle flights [30].

Potter et Whitfield [31] criterion is based on a Reynolds number $R_k = U_k\, k/\nu_k$, in which flow quantities are taken at the altitude k corresponding to the roughness height. Note that this Reynolds number was used in Figure 8 for micron-sized roughness elements. When the smooth wall transition location is known, the Potter and Whitfield criterion provides an estimation of the transition movement as a function of the roughness height.

PANT criterion (Anderson [32]) is based on classical cold supersonic and hypersonic wind tunnel tests conducted during the 'PAssive Nosetip Program', a cold war research program dedicated to improving the design of warheads during the first half of the seventies. PANT criteria uses a parameter:

$$\Psi_1 = R\theta\left(\frac{kTe}{\theta Tw}\right)^{0.7} \quad \text{with} \quad 10^{-2} < \frac{kTe}{\theta Tw} < 10$$

θ is the compressible momentum thickness, $R\theta$ is the Reynolds number calculated with θ. Transition is then predicted where $\Psi_1 = 215$, provided that $\Psi_1 \geq 255$ on the sonic line. Since Ψ_1 is generally an increasing function of x, this imposes that transition always occurs in the subsonic region. Note that PANT correlation is applicable, in principle, for distributed roughness elements. It was modified by Reda [33].

NASA developed several criteria for the Space Shuttle. Reference [34] introduces a wind tunnel transition criterion for smooth wall Space Shuttle in a form $X_T / L = f\left(R\theta/Me\right)$, improved version of the old $R\theta/Me$ = 200 criterion used during the fifties. Here L is the axial length of the vehicle. The roughness effects are introduced in a correlation of R_k with $R\theta/Me$. R_k again is computed with the conditions at the top of the roughness element. In order to simplify computation, it is evaluated at a single reference location X/L = 0.10.

Slightly more recently, a simplified version of the NASA criterion was proposed as :

$$\frac{k}{\delta} = C\frac{Me}{R\theta}$$

Where δ is the physical boundary layer thickness. The constant C needs to be adapted, C=21 for critical and C=35 for effective roughness height. This correlation is specific to the space shuttle geometry, and little is said on its range of validity. In case of other vehicles, it is shown in [35] that the C constant has to be modified according to the geometry and to the numerical tools used for determining boundary layer characteristic parameters.

Re-evaluation of PANT data, combined with space Shuttle conditions, resulted in a new criterion in [30]. Correlation is written :

$$\frac{R\theta}{Me} = 191\left[\frac{k}{\theta}\frac{Te}{Tw}\frac{1}{1+B/B_s}\right]^{-0.444}$$

This correlation is not restricted to transition in the subsonic region. The pressure gradient correction term $\frac{1}{1+B/B_s}$ is not fully defined in the paper.

From this review of transition criteria, there is no unique answer to apply to a flight vehicle. This is mainly due to the fact that the mechanisms leading to boundary layer tripping are not fully understood. A very interesting contribution in this way was provided quite recently by Reshotko et al [36,37,38] who used the transient growth theory to explain the mechanisms of boundary layer tripping and provided an explanation to the famous “blunt body paradox”. (The “blunt body paradox” refers to early 2D transition occurring on spherical forebodies in highly accelerated flow on a cold wall).

6. Conclusion

The problems associated with boundary layer transition in hypersonic flows are numerous and many of them are far from being solved.

On the theoretical point of view, the linear stability theory constitutes a very efficient tool to understand the fundamental mechanisms leading to transition. It can also explain, at least qualitatively, the influence of more or less controlled parameters. The use of non linear PSE helps to model the last stage of the transition process. But the key problem lies in the understanding of the receptivity mechanisms in order to establish the link between the disturbance environment and the initial amplitude of the unstable waves. It is now recognised that streamwise unstable waves are excited by the free stream noise, whilst stationary crossflow unstable waves are generated by micron-sized roughness elements. The sensitivity of crossflow vortices to the surface polishing, however, has to be confirmed and quantified for hypersonic flows.

At the time being, the e^N method is widely used to predict the onset of transition. Of course, this methods presents many shortcomings. Because it is based on linear stability only, receptivity and non linear mechanisms are not taken into account. In addition the non-parallel effects are neglected in the local procedure, and it has been noticed that they could be important for oblique waves. From a practical point of view, the most important issue is the value of the N factor at transition. The problem is particularly complex for 3D flows due to the coexistence of several unstable modes; as the receptivity mechanisms are different, the transition N factors are different.

From a physical point of view, it must be kept in mind that wind tunnel experiments cannot duplicate free flight disturbance environment. Unfortunately, detailed flight results are very difficult to obtain. Although a very large number of flight vehicles has been experimented in the USA over the years, most results were classified for a long time.

Reference [39] mentions over 200 vehicles for flight experiments, used during the cold war era, of which a small fraction has been declassified in these last years. Most of the available data are difficult to analyse, because of a poor knowledge of ambient conditions and of a poor control over the experimental conditions. The scatter in the flight data presented in Figure 2 illustrates this problem. Carefully controlled flight experiments are needed to validate high speed transition theories and prediction methods.

As far as the problem of boundary layer tripping is concerned, one can expect that wind tunnel results are representative of flight conditions, at least for large roughness elements, the effects of which certainly overwhelm those of wind tunnel noise. Nevertheless, there is no "universal" criterion applicable to a large variety of flow conditions. It is hoped that the understanding of the tripping mechanisms will contribute to clarify the situation.

Last but not least, a large amount of work (theoretical, numerical, experimental) remains to be done for introducing the real gas effects in the prediction methods for both "natural" and roughness induced transition.

7. References

[1] Mack L.M.: Boundary layer linear stability theory. In *AGARD Report N° 709*, 1984
[2] Herbert T. Parabolized Stability Equations. In *AGARD Report N° 793*, 1993
[3] Bertolotti F.: Compressible boundary layer analyzed with the PSE equations. *AIAA Paper 91-1637*, 1991
[4] Arnal D.: Boundary layer transition: prediction based on linear theory. In *AGARD Report N° 793*, 1993
[5] Arnal D.: Laminar-turbulent transition problems in supersonic and hypersonic flows. In *AGARD Report N° 761*, 1989
[6] Beckwith I.E., Creel T.R., Chen F.J.and Kendall J.M.: Freestream noise and transition measurements in a Mach 3.5 pilot low-disturbance tunnel. *TP 2180, NASA*, 1983
[7] Chen F.J. and Malik M.R.: Comparison of boundary layer transition on a cone and flat plate at Mach 3.5. *AIAA Paper 88-0411*, 1988
[8] Beckwith I.E.: Development of a high Reynolds number quiet tunnel for transition research. *AIAA Journal, 13(3),* 1975
[9] Malik M.R.: Prediction and control of transition in supersonic and hypersonic boundary layers. *AIAA Journal, 27(11)*, 1989
[10] Schneider S., Skoh C., Rufer S., Matsumara S. and Swanson E.: Transition research in the Boeing/AFOSR Mach-6 quiet tunnel. *AIAA Paper 2002-0302*, 2002
[11] Arnal D., Chanetz B., Carrier G., Coustols E. and Bur R.: State-of-the-art of the "Supersonic Aerodynamics" project at ONERA. *ECCOMAS 2004, Jyvaskyla, Finland*, July 2004
[12] Beckwith I.E., Chen F., Wilkinson S. Malik M. and Tuttle D.: Design and operational features of low-disturbance wind tunnels at NASA Langley for Mach numbers from 3,5 to 18. *AIAA Paper 90-1391*, 1990
[13] Malik M.R., Spall R.E. and Chang C.L.: Effect of nose bluntness on boundary layer stability and transition. *AIAA Paper 90-0112*, 1990
[14] Stetson K.F., Thompson E.R., Donaldson J.C. and Siler L.G.: Laminar boundary layer stability experiments on a cone at Mach 8- Part 2: blunt cone. *AIAA Paper 84-0006*, 1984
[15] Dussillols L.: Calculs de stabilité et transition sur des configurations hypersoniques complexes, *Ph. D. Thesis, SUPAERO, Toulouse*, 1999
[16] Arnal D., Kufner E., Oye I. and Tran P.: Programme TRP Transition: Computational results for transition prediction, *Study Note 7*, March 1996

[17] Perraud J., Arnal D., Dussillols L. and Thivet F.: Studies of laminar-turbulent transition in hypersonic boundary layers at ONERA. *Third European Symposium on Aerothermodynamics for Space Vehicle, Noordwijk, The Netherlands,* 1998
[18] Perraud J., Arnal D. and Thivet F.: Laminar-turbulent transition of hypersonic, chemically reacting boundary layers. *21st Rarefied Gas Dynamics Symposium, Marseille, France*, July 1998
[19] Louis F.: Etude de la transition laminaire-turbulent en écoulement supersonique. *Ph. D. Thesis, SUPAERO, Toulouse,* April 2004
[20] Archambaud J.P., Louis F., Séraudie A., Arnal D. and Carrier G.: Natural transition in supersonic flows: flat plate, swept cylinder and swept wing. *AIAA Paper 2004-2245*, 2004.
[21] King R.A.: Mach 3.5 boundary layer transition on a cone at angle of attack. *AIAA Paper 91-1804*, 1991
[22] Radetsky R.H., Reibert M.S., Saric W.S. and Takagi S.: Effect of micron-sized roughness on transition in swept wing flows. *AIAA Paper 93-0076*, 1993
[23] Tran P., Séraudie A., Wendt V. and Poll D.I.A.: Programme TRP Transition: Experimental results for transition prediction. *Study Note 6*, 1995
[24] Malik M.R. and Balakumar P.: Instability and transition in three-dimensional supersonic boundary layers. *AIAA Paper 92-5049*, 1992
[25] Hanifi A.: Nonlocal stability analysis of the compressible boundary layer on a yawed cone. *Ph. D. Thesis, KTH, Stockholm*, 1995
[26] Cattafesta L.N., Iyer V., Masad J.A., King R.A. and Dagenhart J.R.: Three-dimensional boundary layer transition on a swept wing at Mach 3.5, *AIAA Journal 33(11),* November 1995
[27] Séraudie A., Payry M.J. and Arnal D.: A study of laminar-turbulent transition criteria for hypersonic flow over slender lifting configurations. *Technical Report ONERA/CERT 108/5018.95*, December 1995
[28] Van Driest E.R., Blumer C. and Wells C.S.: Boundary layer transition at supersonic speeds; effect of roughness. *AIAA Journal, Vol 5(10), pp.1913-1915*, 1967
[29] Vignau F.: Etude théorique et expérimentale de la transition en écoulement bidimensionnel compressible. *Ph. D. Thesis, SUPAERO, Toulouse*, 1989
[30] Bouslog S.A., Bertin J.J., Berry S.A. and Caram J.M.: Isolated roughness induced boundary layer transition: Shuttle orbiter ground tests and flight experience, *AIAA Paper 97-0274*, 1997
[31] Potter J.L. and Whitfield J.D.: Effects of slight nose bluntness and roughness on boundary layer transition in supersonic flows. *J. Fluid Mech., Vol 12(4), pp.501-535*, 1962
[32] Anderson A.D.: PAssive Nosetip Technology (PANT) program. Interim report, Volume X, Appendix A: Boundary layer transition on nosetips with rough surfaces. *SAMSO-TR-86,* January 1975
[33] Reda D.C.: Correlation of nosetip boundary layer transition data measured in ballistics-range experiments, *AIAA Paper 80-0286* and *Sandia National Labs. Rep SAND-79-0649*, November 1979
[34] Bertin J.J., Hayden T.E. and Goodrich W.D.: Comparison of correlations of shuttle boundary layer transition due to distributed roughness, *AIAA Paper 81-417*, 1981
[35] Liechty D.S., Berry S.A. and Hollis B.R.: Comparison of methods for determining boundary layer edge conditions for transition correlation. *AIAA Paper 2003-3590*, 2003
[36] Tumin A. and Reshotko E.: Optimal disturbances in compressible boundary layers. *AIAA Paper 2003-0792*, 2003
[37] White E.B. and Reshotko E.: Roughness induced transient growth in a flat plate boundary layer. *AIAA Paper2002-0138*, 2002

[38] Reshotko E. and Tumin A.: The blunt body paradox. A case of transient growth. *IUTAM Symp. on Laminar-Turbulent Transition, Sedona, AZ, September 1999, Springer-Verlag, H.F. Fasel and W.S. Saric editors*, 2000
[39] Schneider S.P.: Flight data for boundary layer transition at hypersonic and supersonic speeds. *Journal of Spacecraft and Rockets, Vol. 36(1), pp.8-20*, 1999

PART B. SHOCK WAVE/BOUNDARY LAYER INTERACTION

1. Introduction

The flow past a hypersonic vehicle is the seat of strong shock waves forming ahead of the vehicle nose, the rounded leading-edge of wings and tails, at the air-intake compression ramps of an air-breathing propulsion system, at the control surfaces, at the rear part of an afterbody where the nozzle jets meet the outer stream, to name the most salient examples. These shock waves are the main cause of heating and are at the origin of interferences resulting from their intersections and interactions with the boundary layer developing on the vehicle surface. Because of their dramatic importance, such strong viscous interactions have been extensively studied during the past 50 years and are still the subject of active research due to their complexity and the difficulty to predict them especially in turbulent regime [1-4]. Shock wave/boundary layer interactions (SWBLIs) can induce separation which causes loss of a control surface effectiveness, drop of an air intake efficiency and may be at the origin of large scale fluctuations such as air-intake buzz, buffeting or fluctuating side loads in separated propulsive nozzles. In high enthalpy flows, the subsequent reattachment on a nearby surface of the separated shear layer gives rise to local heat transfer rates which can be far in excess of those of an attached boundary layer [5].

The large amount of experimental results on shock wave/boundary layer interaction in 2D flows has allowed a clear identification of the role played by the main parameters involved in the interaction process. Also correlation laws have been deduced giving the upstream interaction length, the limit for shock induced separation and, of prime importance in hypersonic flows, the peak heat transfer at reattachment. The situation is not so satisfactory in 3D flows because of the difficulty to establish a clear physical description of the flow organisation. In addition, the calculation cost of 3D flows renders even now their prediction far more difficult than that of 2D or axisymmetric interactions.

Although the vast majority of configurations in the real world are three-dimensional, this Lecture is focussed on the specific features of hypersonic SWBLIs in 2D and/or axisymmetric flows, which is sufficient to identify the influence of the key parameters involved in hypersonic interactions. Examination of 3D configurations raises complex topological questions whose consideration would take too much space (For information on 3D SWBLIs, see [6-9]).

The consequences of high Mach number and enthalpy levels, typical of hypersonic flows, are multiple:

1. Due to large differences in temperature within the flow field, adiabatic wall conditions are rarely reached, hence a specific effect of wall temperature.
2. Because of the large temperature variation in the dissipative regions, density undergoes a large decrease in the boundary layer, hence an amplification of the displacement effect which, in conjunction with the pressure-deflection dependence, leads to strong viscous/inviscid coupling effects.
3. The shock waves forming in the flow are very intense and interact strongly with the boundary layers giving rise to a further amplification of the viscous effects.
4. In truly hyperenthalpic flows, the heating caused by shocks affects the gas thermodynamic properties, the resulting real gas effects influencing the interacting flow.

5. The shock forming ahead of a hypersonic vehicle being both intense and highly curved, the vehicle is surrounded by a layer of rotational fluid or entropy layer which affects the boundary layer development and its further interaction with a shock wave.
6. The conjunction of high Mach number and low density at high altitude tends to maintain a laminar regime over a great part of the vehicle surface. Thus, situations are encountered where SWBLIs are laminar or transitional, the pressure gradients associated with the interaction tending to precipitate the laminar-boundary layer transition.
7. The strong coupling between the interaction and the flow inviscid part induces shock waves which interfere between them to generate complex shock patterns.

As a consequence of theses features, computation of hypersonic SWBLIs raises difficult problems which are still largely unsolved. The Lecture is devoted to a physical description of the physics of SWBLIs from our present knowledge of these phenomena and provides guides to cope with practical problems. The modelling aspects will be briefly addressed due to the limited extent of this text and of the lack of definitive conclusions in this field.

2. Shock wave/boundary layer interaction properties

2.1 General considerations: The basic interactions

The three basic interactions between a shock wave and a boundary layer are the ramp flow, the impinging reflecting shock, and the pressure discontinuity resulting from adaptation to a higher downstream pressure level (see Figure 1). The first case corresponds to a control surface or an air-intake compression ramp, the second to shock reflection inside an air intake of the mixed supersonic compression type, the third to the condition at the exit of an over-expanded nozzle.

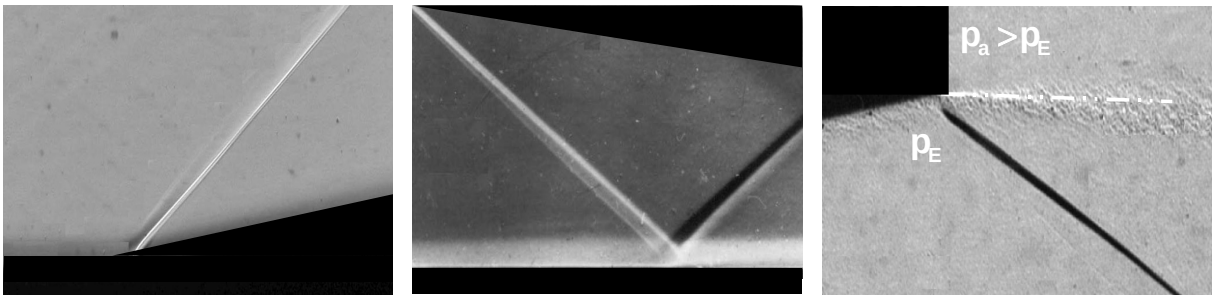

a – ramp flow *b – incident-reflecting shock* *c – adaptation shock*

Figure 1. The three basic shock wave/boundary layer interactions

1. In the ramp flow, an abrupt change in the wall inclination is the origin of a shock through which the incoming flow undergoes a deflection equal to the wedge angle α.
2. The second flow type is the impingement on a wall of an incident shock (C_1). Now the incoming flow undergoes a deflection $\Delta\varphi_1$ through (C_1), the necessity for the downstream flow to be again parallel to the wall entailing the formation of a reflected shock (C_2), the deflection through (C_2) being $\Delta\varphi_2 = -\Delta\varphi_1$.
3. In the third case, the shock wave is provoked by a pressure jump with a subsequent deflection $\Delta\varphi$ of the flow, whereas in the previous cases the pressure jump results from a flow deflection. In what follows we will not consider the last case which pertains to

specific problems of nozzle adaptation, although some general SWBLI properties are pertinent to this case.

In the following sections we will consider indifferently the physical properties of shock wave/boundary layer interaction produced either by a ramp or an impinging shock, the behaviour, or response, of the boundary layer being similar in the two cases as illustrated in Figure 2 showing laminar Navier-Stokes calculations. Laminar and turbulent interactions will be examined in a unified manner since there are not basic differences between the two regimes as far as the overall flow topology is concerned. Of course, turbulent interactions differ from laminar interactions in terms of scales, intensity of pressure rise and thermal effects (heat transfer for example). Such differences will be pointed out in what follows.

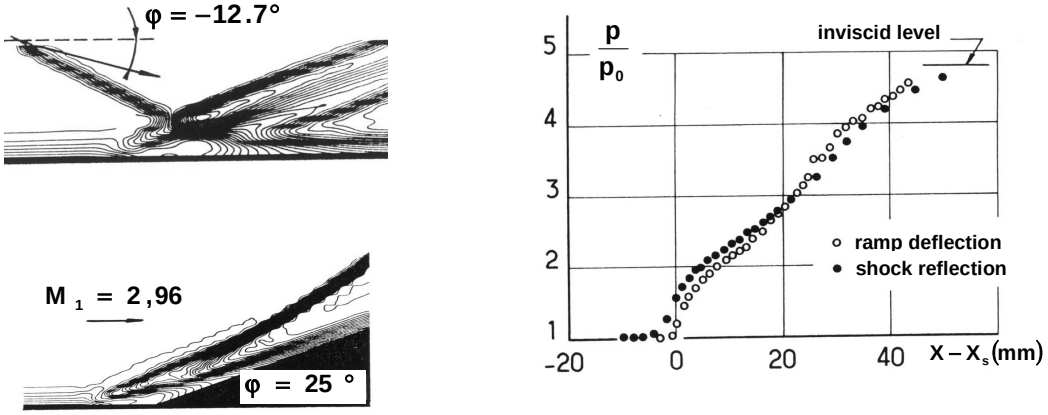

Figure 2. Ramp deflection and shock reflection in laminar flow [10]

2.2 The compression ramp flow

When the ramp angle α is small, the overall flow structure is not much affected by the interaction taking place at the ramp origin. The main difference is a spreading of the wall pressure distribution, the step of the inviscid solution being replaced by a progressive rise between the upstream level p_0 and the final value p_1 corresponding to the oblique shock equations. The spreading of the wall pressure distribution denotes the upstream influence mechanism through which the presence of the shock is felt upstream of its origin in perfect fluid; i.e., the ramp apex. This effect is quantified by the upstream interaction length L_u defined as the distance between the interaction onset (where the wall pressure distribution starts to rise) and the ramp origin or the incident shock impact point in the inviscid flow model. As shown in Figure 3, this upstream propagation results from the existence of a subsonic layer in the boundary layer inner part through which any signal (a pressure change) is propagated both in the upstream and downstream directions. The compression associated with the shock causes a progressive dilatation of the subsonic channel inducing in the supersonic contiguous part of the flow compression waves which coalesce to constitute the ramp induced shock at some distance from the wall. In a turbulent boundary layer, the subsonic channel is extremely thin so that this shock forms within the boundary layer which behaves like an inviscid rotational fluid over most of its thickness. The interaction is said a rapid interaction process in which viscous forces play a negligible role compared to the action of pressure and momentum terms. However, because of the no-slip condition, to avoid

inconsistencies a thin viscous layer in contact with the wall must be considered. The interacting flow manifests a triple-deck structure with an outer irrotationnal deck, a non viscous but rotationnal middle deck and a viscous inner deck [11,12].

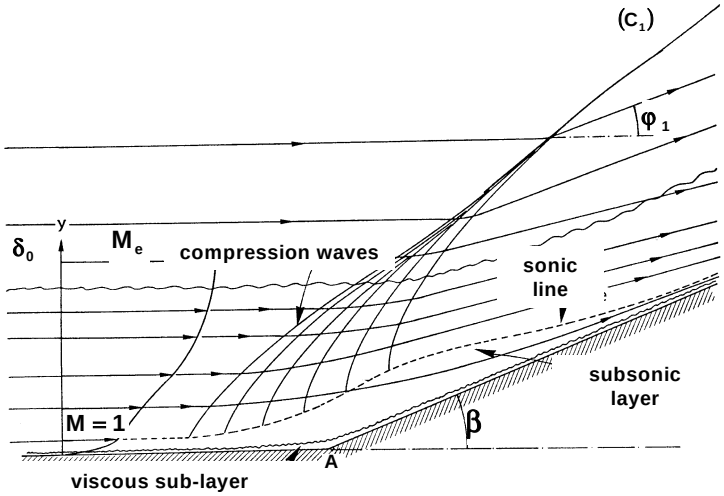

Figure 3. The structure of a ramp flow without boundary layer separation

At high Mach and Reynolds numbers, the velocity profile of a turbulent boundary layer is so filled that the subsonic layer is excessively thin. Then, as shown in Figure 4, the shock originates from a region very close to the wall and propagates in the boundary layer where it is bent because of the Mach number variation.

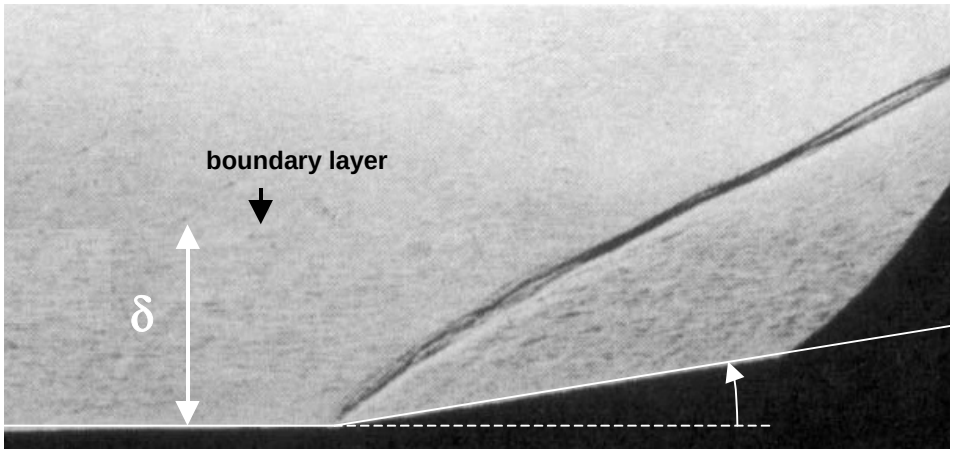

Figure 4. Turbulent ramp flow without separation at high Mach and Reynolds numbers [13]

When the ramp angle α is raised (hence the shock strength), the upstream influence distance increases accordingly and a situation can be reached where the pressure rise is high enough to induce separation of the boundary layer (see Figure 5). In this situation:

1. The ramp upstream influence, hence upstream influence length L_u, has considerably increased. A new scale is introduced as the separation length L_S which separates the separation point from the ramp origin or incident shock theoretical impact point.
2. A first shock associated with separation forms well upstream of the ramp.
3. A second shock originates from the reattachment region on the ramp which intersects the separation shock at a short distance from the wall at high Mach number.

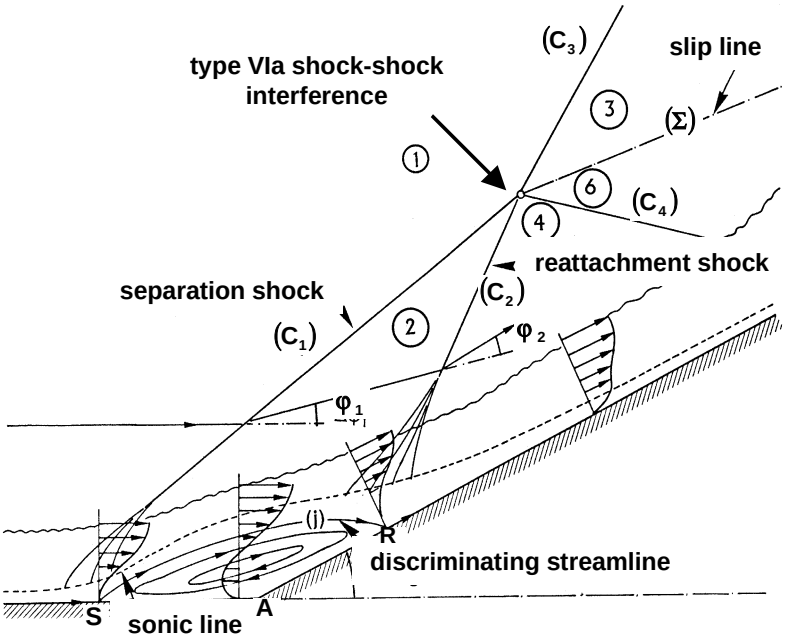

Figure 5. The structure of a ramp flow with boundary layer separation

Separation and reattachment being progressive, the induced compression waves coalesce into shocks at some distance from the wall. However at high Mach number, the coalescence is so rapid than the separation and reattachment shocks form within the boundary layer and seem to originate from the wall. Frequently, the shock pattern tends to be embedded within the boundary layer as shown in Figure 6.

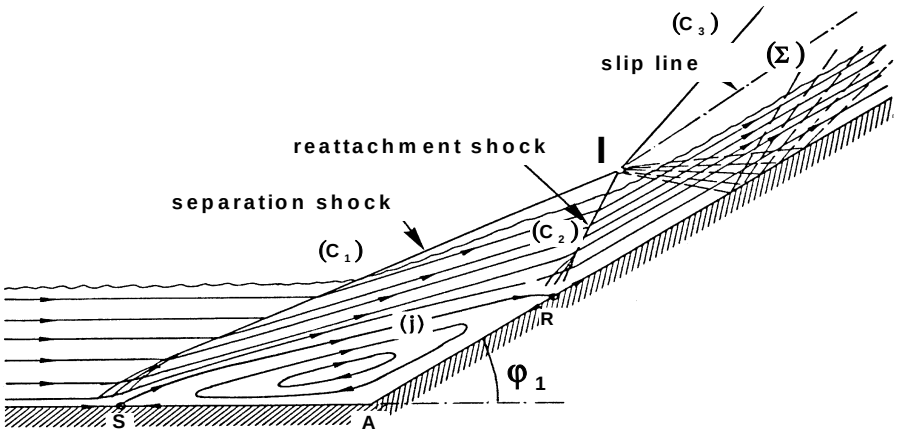

Figure 6. Ramp flow with boundary layer separation at high Mach number

Intersection of the separation and reattachment shocks produces a type VIa shock-shock interference pattern [5,14]. As soon as the Mach number is greater than about 2, a centred expansion emanates from the triple point *I* where the two shocks meet in order to make the flows above and below the triple point compatible. In hypersonic flows, this expansion is so closes to the wall that it induces an important pressure decrease when striking the wall (see Section 2.5). The shadowgraphs in Figure 7 give examples of turbulent hypersonic interactions at a compression ramp in a Mach 9.22 hypersonic flow.

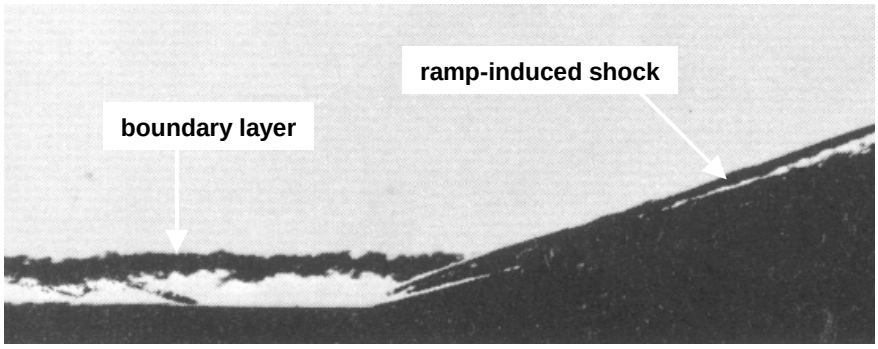

a – interaction without separation

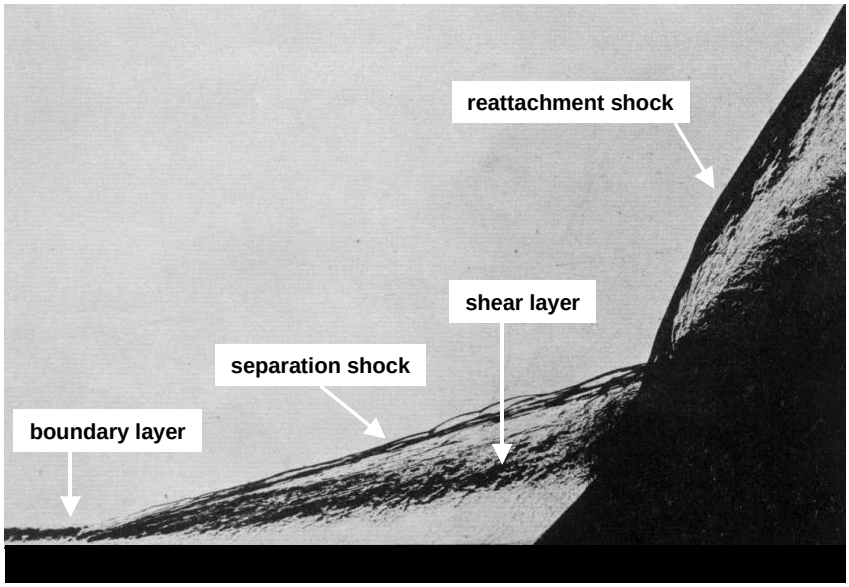

b – interaction with separation

Figure 7. Shadowgraph of turbulent ramp flows at Mach 9.2 [15]

In the separated case, a shear layer develops between the outer stream, below the separation shock, and the "dead air" region in contact with the wall. This shear layer is a key feature of separated flows. Along it, the low speed flow resulting from separation is accelerated under the action of viscous forces (true viscosity or turbulent eddy viscosity) until it reaches a momentum level enabling it to overcome the second pressure rise at reattachment. Since the pressure rise at separation depends only of the flow upstream conditions (see the *free interaction theory* below) any increase of the overall pressure rise results in a higher pressure rise at reattachment. This involves an upstream displacement of the separation point

in order to permit a longer acceleration phase (or mixing length) of the fluid in the shear layer. The shear layer impacting the ramp under a large angle, the situation at reattachment is similar to that at a front stagnation point, hence very large local heat transfer rates, the (average) stagnation temperature in the shear layer being comparable to that of the outer flow.

The difference in scales between laminar and turbulent ramp flows with separation is illustrated in Figure 8. The laminar interaction was obtained at Mach 10 in a low Reynolds number facility allowing to maintain the laminar regime throughout the interaction. The visualisation was made with the electron beam fluorescence technique. The turbulent case corresponds to an interaction at Mach 8.6, the picture being a short exposure time shadowgraph. For the laminar interaction, the streamwise extent is of the order of several boundary layer thickness, whereas it is here less than one boundary layer thickness for the turbulent case.

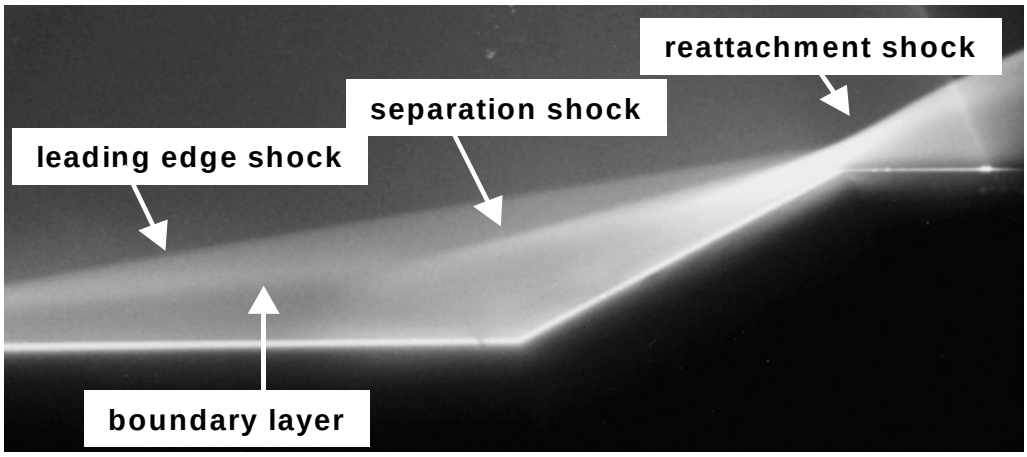

a – laminar interaction at a cylinder-flare junction [16]

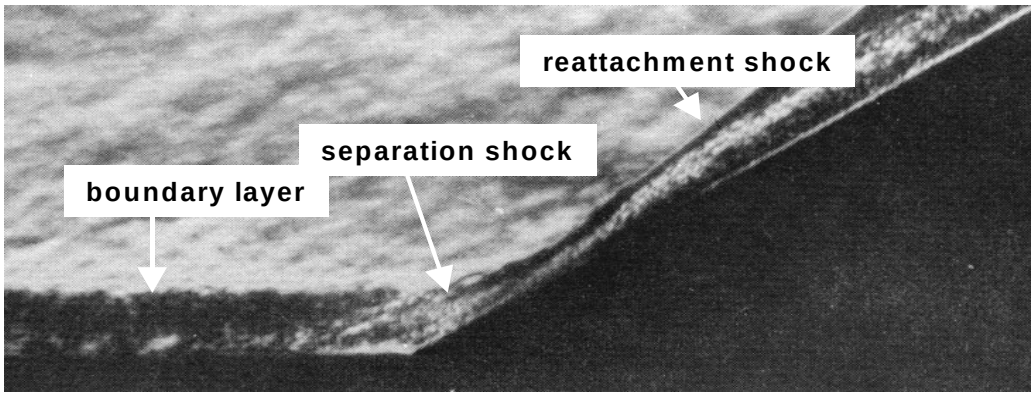

b – turbulent ramp flow [17]

Figure 8. Laminar and turbulent interactions

2.3 The impinging-reflecting oblique shock

In the present case, a planar oblique shock strikes a wall facing the obstacle having provoked the shock. As shown in Figure 9, penetration of the incident shock into the boundary layer generates a complex wave pattern resulting from its refraction through the rotational and supersonic nearly parallel flow constituted by the major part of the boundary layer.

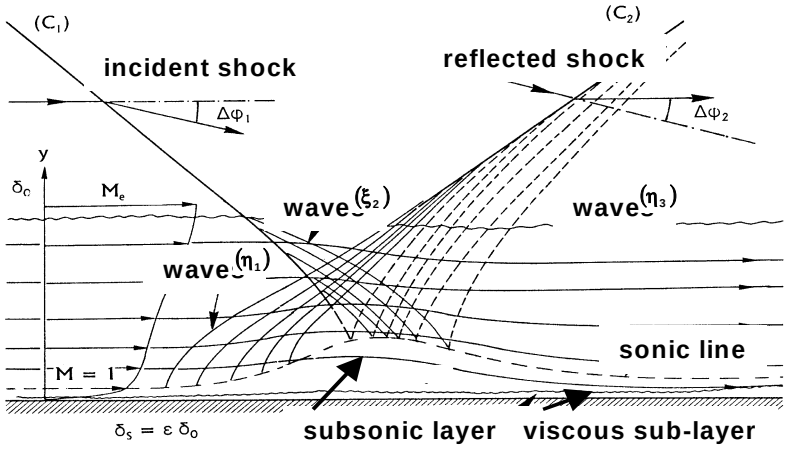

Figure 9. Impinging-reflecting shock without separation

As in the previous situation, the existence of a subsonic inner layer allows the upstream propagation of the shock influence. When separation occurs, the separation shock meets the incident shock at some distance from the wall giving rise to a type I shock-shock interference as shown in Figure 10. The sequence of shadowgraphs in Figure 11 visualises the shock reflection for increasing values of the primary deflection through the incident shock in the case of a turbulent interaction at high Mach number. Conclusions similar to those pertaining to the wedge flow can be drawn. In particular one notes the small angle of the reflected shock with respect to the surface. In this case the shock pattern associated with the interaction is almost entirely embedded within the boundary layer.

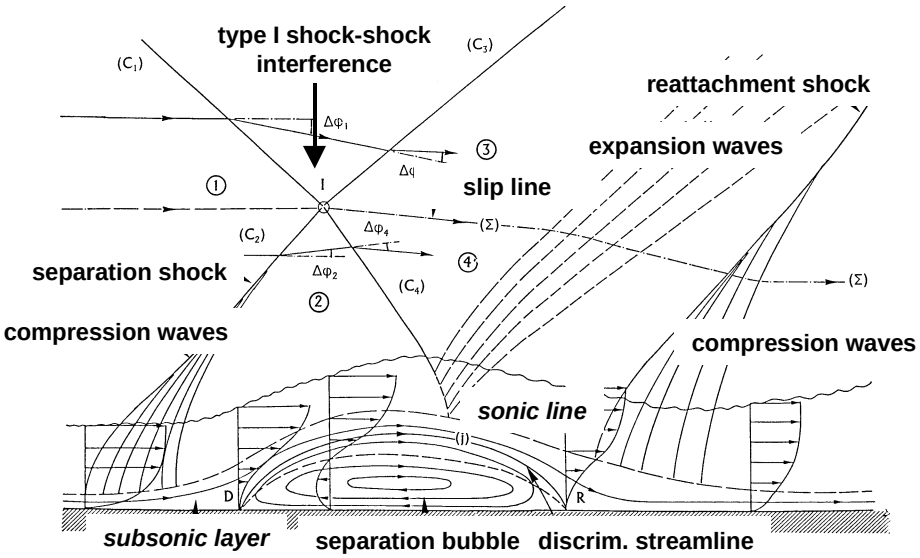

Figure 10. Impinging-reflecting shock with extended separation

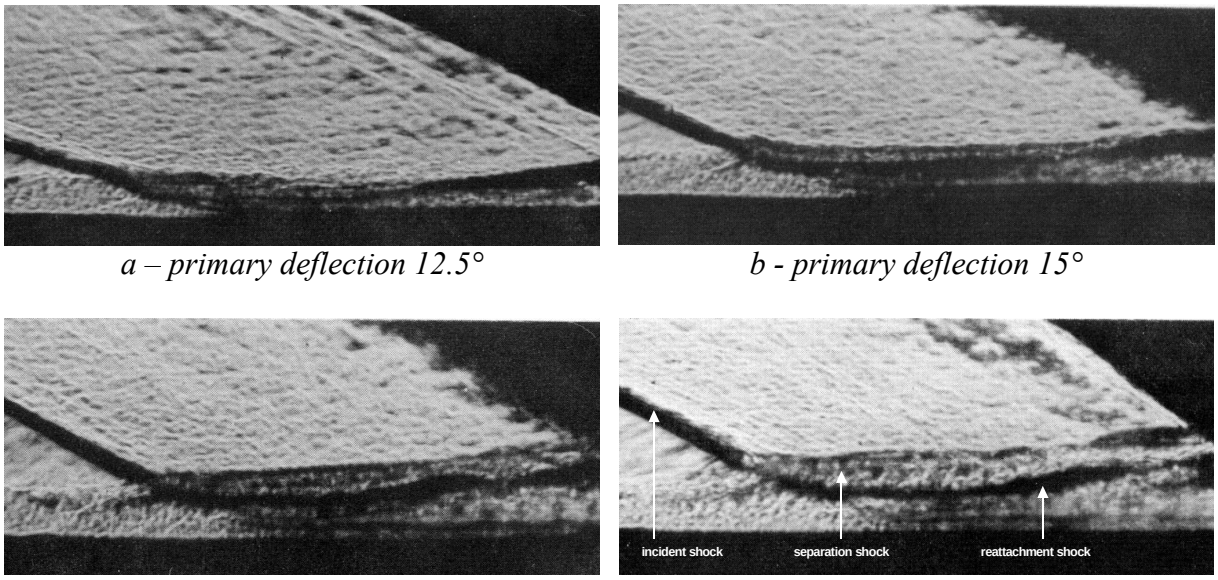

a – primary deflection 12.5° *b - primary deflection 15°*

c – primary deflection 17.5° *d – primary deflection 19.8°*

Figure 11. Shadowgraphs of impinging-reflecting shock at Mach 8.6 [17]

In either of the above situations, when the shock is strong enough to separate the boundary layer, the resulting structure of the inviscid outer stream strongly depends on the boundary layer development in the interaction region. There is a dramatic change in the shock pattern with formation of several shocks whose intersection generates refracted and transmitted shocks, expansion waves and slip lines. This fact leads to severe difficulties in the modelling of the interaction, a good prediction requiring an accurate capture of this waves and discontinuities. In addition, in hyperenthalpic flows, the sensitivity of the shock system to the gas thermodynamics (the so-called real gas effects) may have large impact on the interacting flow (see Section 2.7).

2.4 Supersonic separation and the free interaction theory

The behaviour of the flow during separation at supersonic Mach number can be interpreted by the free interaction theory, even though some aspects of the phenomenon do not fit with this simple theory, particularly for turbulent interactions [18]. This theory establishes that the pressure rise during separation of a supersonic boundary layer satisfies the relation:

$$\frac{p - p_0}{q_0} \propto \left(C_{f_0}\right)^{-1/2} \left(M_0^2 - 1\right)^{-1/4}$$

where q_0 is the dynamic pressure of the incoming flow, M_0 the Mach number and C_{f_0} the skin friction coefficient at the interaction origin. The interaction L streamwise extent obeys a law of the form:

$$L \propto \delta_0^* \left(C_{f_0}\right)^{-1/2} \left(M_0^2 - 1\right)^{-1/4}$$

where δ_0^* is the incoming boundary layer displacement thickness. For hypersonic flows, the following equivalent expression can be derived:

$$\frac{L}{\delta_0^*} \propto \frac{(M_0\,\alpha)^2}{\bar{\chi}_0}$$

where $\bar{\chi}_0 = M_0^3 / \sqrt{R_{x0}}$ is the hypersonic interaction parameter.

The free interaction theory shows that during separation the pressure rise and interaction extent depend only of the flow properties at the interaction onset. Since the skin friction coefficient decreases when the Reynolds number increases, the free interaction theory predicts an increase of the interaction extent and a decrease of the total pressure rise when the Reynolds number is increased. The consequence is that separation requires a stronger shock at low than at high Reynolds number. This behaviour is verified in laminar flows but is in contradiction with observation in turbulent flows as soon as the Reynolds number R_δ is greater than 10^5: Beyond this limit a turbulent boundary layer offers a greater resistance to separation when the Reynolds number is further increased [13,19,20] The behaviour of a boundary layer results from a struggle between viscous and inertia forces (i.e., pressure and momentum), the two having opposite influences. The free interaction theory privileges the viscous forces since it involves only the properties at the wall through the skin friction coefficient, hence its correct prediction in low Reynolds number flows. In high Reynolds number turbulent flows ($R_\delta > 10^5$), the inertia terms predominate causing the tendency reversal observed in turbulent flow. A clear perception of the conflict between viscous and inertia terms is essential for the understanding of flow behaviour in strong interaction with separation, this aspect being hidden in the global approach based on the solution of the Navier-Stokes equations.

For practical application, the limit for shock induced separation is of major concern since it places a limit to the maximum strength of a reflecting shock or the maximum deflection angle of a control surface. This limit is most often defined in the plane of two variables: the ramp angle α (or equivalent angle for shock reflection) and the Reynolds number R_δ, a different curve corresponding to each value of the Mach number M_0. As a consequence of the above remarks, for a given upstream Mach number, the shock strength required to separate the boundary layer decreases when the Reynolds number increases. Above, $R_\delta = 10^5$ in turbulent flow a trend reversal occurs, the limit shock strength increasing with the Reynolds number. In reality, this increase is modest, the limit for shock induced separation depending then only of the Mach number. At fixed Reynolds number, the shock intensity entailing separation increases with the Mach number (for details and practical information, see [1]).

2.5 Features of the wall pressure distribution

In high Mach number flows, the wall pressure distribution is characterised by a sharp rise due to the high pressure ratio across the shock wave. As shown in Figure 12, the pressure distribution exhibits the following features:

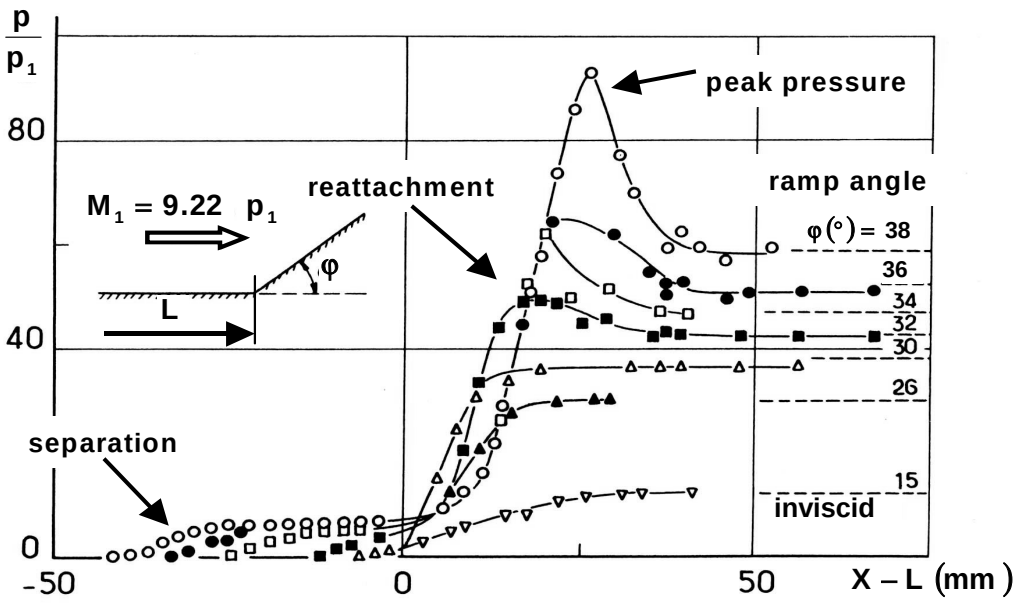

Figure 12. Wall pressure distributions in a turbulent ramp flow at Mach 9.22 [15]

1. For moderate ramp angle ($\alpha < 26°$) the shape of the pressure curve does not differ much from that observed at smaller Mach numbers.
2. Existence of separation is denoted by a pressure plateau whose streamwise extent increases with the shock intensity.
3. The pressure rise associated with separation remains unchanged when the separation point moves upstream as a consequence of the ramp angle increase. Since, as shown by the free interaction theory (see above) the pressure curve at separation is entirely determined by the flow properties at the interaction onset, the sole effect of a rise in the overall pressure jump is to provoke an extension of the plateau pressure.
4. Once separation has occurred, there is a large asymmetry between the pressure rises at separation and reattachment, the latter being much more ample. As the pressure rise to separation does not depend on downstream conditions, an increase of the total pressure rise entails a higher pressure rise at reattachment. This can only be achieved by an increase in the maximum velocity on the streamline stagnating at the reattachment point R (see Figure 10), hence an increase of the shear layer length according to the mechanism explained in Section 2.2.
5. When $\alpha > 30°$, the pressure distribution exhibits a peak in the reattachment region followed by a fall and the tendency towards the inviscid solution level, the overshoot at reattachment being higher when the wedge angle is increased. This phenomenon, observed when the flow is separated is associated to the type VIa interference between the separation and reattaching shocks (see Section 2.2). An examination of the case $\alpha = 38°$ in Figure 12, shows that the deflection angle at separation is $\approx 10°$ which leads to a pressure ratio ≈ 6.23 for an upstream Mach number $M_0 = 9.22$. The remaining deflection at reattachment being $28°$, their results a pressure ratio ≈ 17.3, hence a total pressure ratio ≈ 109. For a unique oblique shock at Mach 9.22 with a deflection of 38°, the pressure jump being equal to 58.7, an expansion must start from the triple point to equalise the downstream pressures.

2.6 Thermal effects in hypersonic interactions

The high enthalpy level of the outer flow, typical of truly hypersonic conditions, has three major consequences on SWBLIs:

1. When the wall temperature is well below the outer stream stagnation temperature a cold wall situation exists which may significantly affect the interaction properties.
2. Heat transfer processes take a dramatic importance, especially in separated flows where the shear layer emanating from the separation region impacts the reattachment surface.
3. As already pointed out, real gas effects modify the thermodynamic and transport properties of the gas in a way that may influence the interaction.

The first two effects are well characterised by a wealth of experimental results, information on the third effect being more scarce.

2.6.1 Wall temperature effects on the interaction properties

The wall thermal condition is characterised by the ratio of the wall temperature T_w to the recovery temperature T_r corresponding to adiabatic conditions. Most hypersonic applications correspond to cold wall situation since the outer stream temperature is higher than the surface temperature of the vehicle. During a re-entry, the surface temperature rises and can be close to the recovery temperature so that thermal protections are needed to prevent heat from reaching the structure. The main concern of hypersonic vehicle design is thus to predict the heat transfer at the wall in order to properly size the thermal protection or the cooling system in the case of rocket engine. The general effect of wall cooling on a laminar interaction is to contract the interaction domain as demonstrated by experiments on ramp type or hollow-cylinder-plus-flare type models. In wind tunnel experiments, representative T_w / T_{st_0} ratios are achieved by cooling the model with circulation of liquid nitrogen (T_{st_0} is the outer stream stagnation temperature). As shown in Figure 13, wall cooling contracts the interaction domain, compared to the adiabatic case. This tendency was confirmed by experiments with a model which could be cooled or heated, thus allowing a clear identification of the wall temperature effect [23]. In turbulent flows, wall cooling has also the effect to contract the interaction domain as shown in Figure 14 where the separation length L_S scaled to its value in the adiabatic case is plotted as function of T_w / T_r for different ramp angles. On the other hand, it was found that a rise in wall temperature above the recovery temperature induces an extension of the interaction which is consistent with the above findings [24].

There is not a unique explanation to the decrease in L with the wall temperature. This tendency is in agreement with the free interaction theory, since a lowering of the wall temperature provokes an increase of the skin friction coefficient and a reduction of the boundary layer displacement thickness (due to an increase of density) hence a contraction of L. However, the observed dependence on wall temperature is beyond that predicted by the free interaction theory and an improved law was proposed to better correlate the wall temperature effect in laminar flow [25]. The contraction of the interaction domain can also be explained by a the thinning of the boundary layer subsonic channel due smaller sound velocity at low temperature entailing a higher Mach numbers close to the wall.

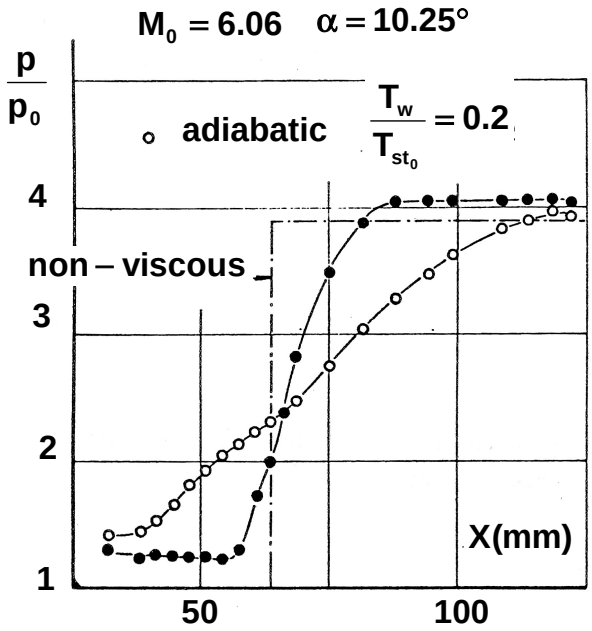

Figure 13. Effect of wall cooling on wall pressure distribution for a laminar ramp flow [21]

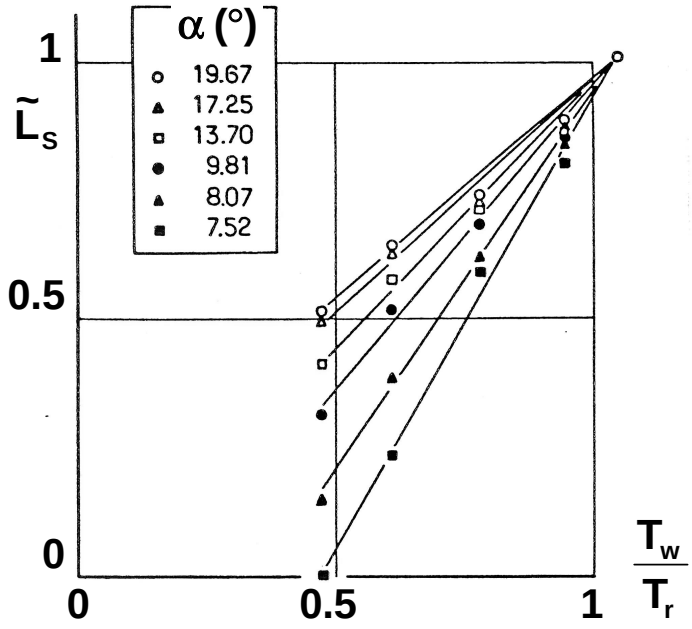

Figure 14. Effect of wall cooling on turbulent separation length [22]

2.6.2 Heat transfer in hypersonic interactions

The surface heat transfer is represented via the Stanton number usually defined as:

$$S_t = \frac{q_w}{\rho_e u_e (h_r - h_w)}$$

where q_w is the wall heat transfer (in W/m^2), ρ_e and u_e are the density and velocity at the boundary layer edge, h_w the gas enthalpy at the wall and h_r the recovery enthalpy (corresponding to the adiabatic case). Because these quantities are difficult to determine in hypersonic interactions, it is more usual to use a Stanton number defined by:

$$\bar{S}_t = \frac{q_w}{\rho_\infty u_\infty (h_{st_\infty} - h_w)}$$

where ρ_∞ and u_∞ are the density and velocity of the upstream flow and h_{st_∞} its stagnation enthalpy. If the gas is assumed calorically perfect, then:

$$\bar{S}_t = \frac{q_w}{\rho_\infty u_\infty C_p (T_{st_\infty} - T_w)}$$

The salient feature of hypersonic SWBLIs is the existence of extremely high heat transfer rates in the interaction region when separation takes place (see Figure 15). This problem, which is crucial for the sizing of thermal protections, has been studied by many investigators both in laminar and turbulent flows. Heat transfer rates are particularly intense in the vicinity of the point where the separated flow reattaches, the peak in heat transfer being associated with the stagnation at *R* of the shear layer developing from the separation point (see Figure 7). The situation at *R* is similar to a nose stagnation point with the difference that the flow impinging on the ramp (control surface) has been compressed through a succession of oblique shocks at separation and reattachment instead of a unique normal shock, hence a far less important loss in stagnation pressure (or smaller entropy rise). Since:

$$\rho_e u_e \propto \frac{p_{st_e}}{\sqrt{T_{st_e}}}$$

where p_{st_e} and T_{st_e} are relative to the flow at the boundary layer edge in the interacting region, we see that the heat transfer process will be far more efficient than at the vehicle nose.

The heat transfer distribution measured on a cylinder-flare model in a Mach 10 flow at low Reynolds number is shown in Figure 16, the flow remaining laminar throughout the interaction domain. The curve shows that the heat transfer decreases slowly in the most upstream part of the cylinder, in agreement with the strong/weak viscous interaction theory. A faster decrease starts at a location coincident with separation onset. This decrease is typical of shock induced separation in laminar flows. Heat transfer goes to a minimum in the separated region; then it increases sharply at reattachment, the peak value being reached slightly downstream of the reattachment point.

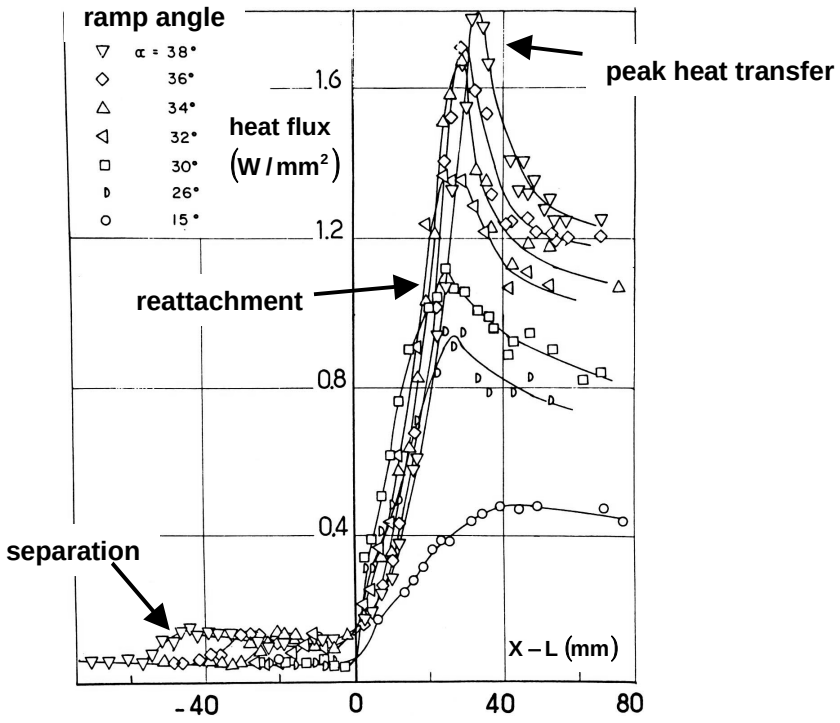

Figure 15. Wall heat transfer distribution in a turbulent Ramp flow at Mach 9.22 [15]

A heat transfer distribution in a ramp-induced interaction corresponding to a higher Reynolds number is plotted in Figure 17. This result is relative to $M_\infty = 10$ and $T_w / T_r = 0.3$, the model being a 15° ramp fixed on a flat plate with sharp leading edge. In this experiment the boundary layer is laminar over the major part of the interaction but transition occurs in the reattachment region which leads to a more important heat transfer rise at reattachment. The fact that the wall heat transfer decreases at separation proves that the flow is laminar until separation and that the transition process starts in the shear layer before its impact with the ramp.

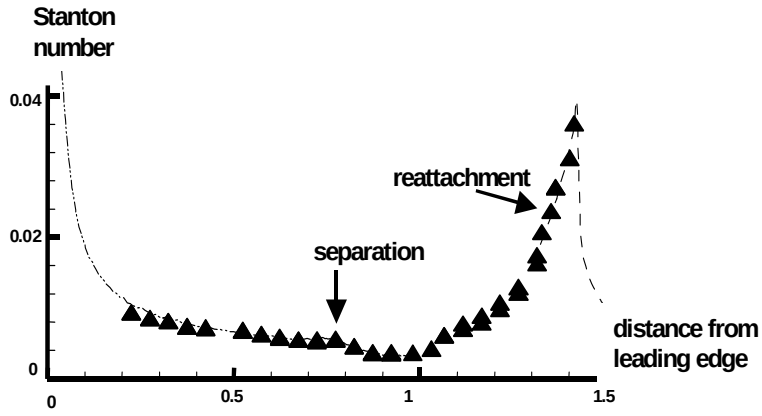

Figure 16. Heat transfer distribution in a fully laminar SWBLI [26]

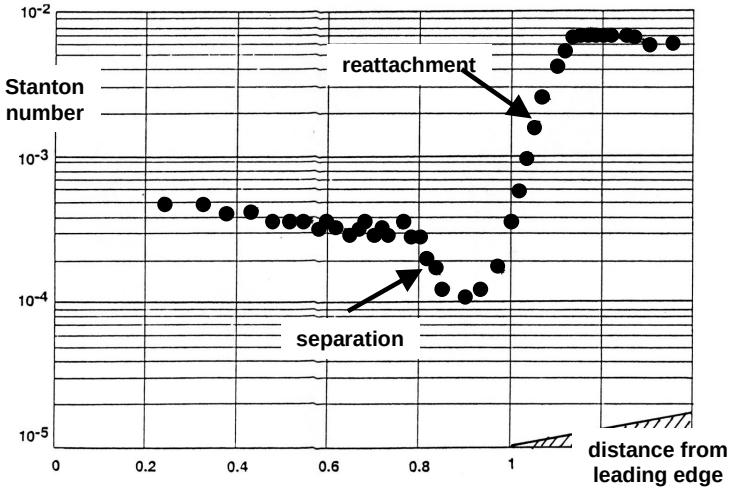

Figure 17. Heat transfer distribution in a transitional SWBL [27]

Results relative to a fully turbulent interaction at $M_\infty = 5$ produced by a 35° ramp are plotted in Figure 18. Although the Mach number is modest, these results are similar to those obtained at higher Mach numbers. In this case, the heat transfer first slowly decreases in the upstream part of the flat plate and then rises well upstream of the ramp hinge line. This first rise followed by a slow decrease can be attributed to laminar-turbulent transition. A second rise takes place at the separation location, this behaviour opposite to that observed in laminar flows being typical of turbulent shock-induced separation. Further downstream, the heat transfer sharply rises during reattachment to a peak value downstream of the reattachment point. The heat transfer rise at separation is explained by the turbulence amplification in the vicinity of the separation point and further downstream. The large eddies which then form promote exchanges between the wall region and the outer high enthalpy flow, leading to a rise in heat transfer.

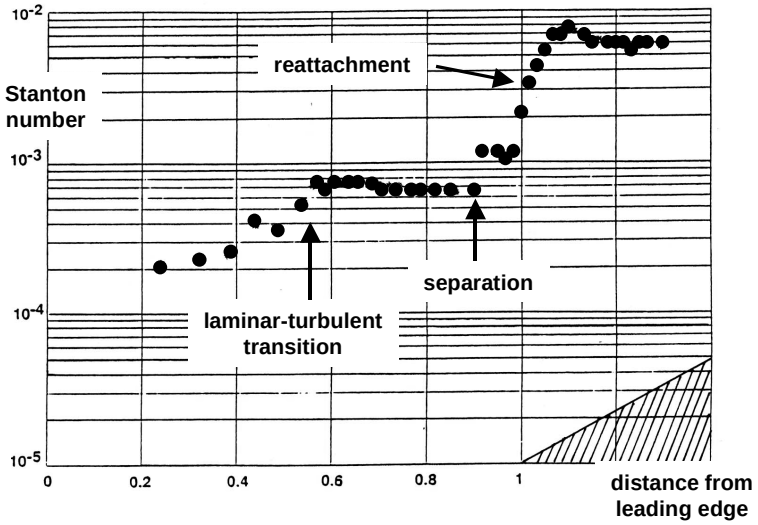

Figure 18. Heat transfer distribution in a fully turbulent SWBLI [27]

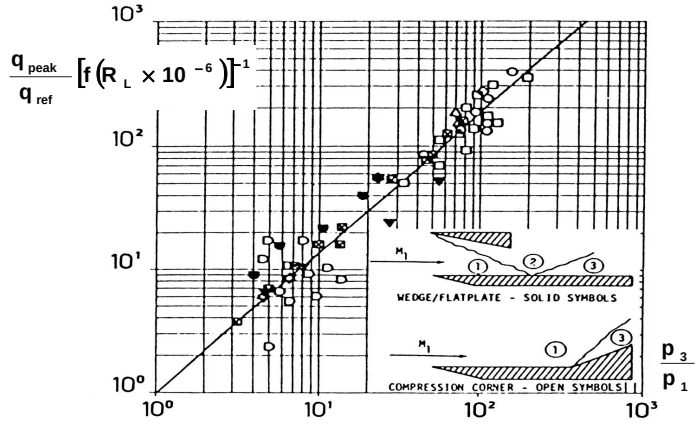

a – laminar flow

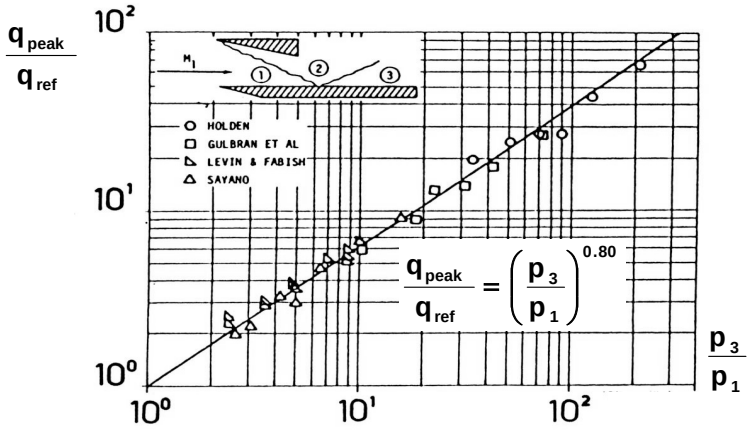

b – turbulent flow

Figure 19. Empirical peak heat transfer correlations in a SWBLI [28]

Peak heat transfer prediction is still a challenging task because of the lack of realistic turbulence models and of the difficulty to accurately compute a flow field with so high gradients. For practical applications, the empirical correlations given in Figure 19 can be of great help. They provide the peak value of the heat transfer, divided by the heat transfer in the absence of interaction at the same location and for the same general conditions, as function of the total inviscid pressure ratio throughout the interaction.

2.7 Real gas effects on shock wave/boundary layer interaction

In hypervelocity conditions, the flow past the vehicle exhibits real gas effects due to the vibration, dissociation and ionisation provoked by the passage of air through the strong bow shock. A subsequent interaction will thus involve a gas whose composition and physical properties may be greatly modified compared to an non-dissociated gas. We are in a situation where real gas effects are coupled with strong viscous/inviscid interactions. If the calorically perfect gas (i.e., a gas with constant ratio of specific heats throughout the flow field) is taken as a benchmark, real gas or chemical effects will be felt at two stages:

1. Since the thermodynamic properties are not the same, the structure of the inviscid part of the flow is modified as compared to the constant γ case.
2. The transport properties (viscosity, heat conduction and diffusion coefficients) are affected by dissociation and chemical phenomena, which has consequences on the flow viscous part.

Thus, non equilibrium vibrational excitation and chemical reactions may affect the separated length through a change in shock angle (inviscid flow effect) and in the incoming boundary layer thickness (viscous effect).

As compared to the perfect gas case, there are few convincing experimental results about the incidence of real gas effects on SWBLI. Basic experiments on these effects have to be executed in high enthalpy facilities which are both rare and costly to operate. In addition, it is difficult to perform parametric investigations in such facilities, running at high enthalpy conditions entailing changes in the other flow parameters. In such circumstances, it is delicate to establish a clear identifications of the sole real gas effects. Information must be obtained from computations of laminar interactions to exclude the difficult question of turbulence modelling [29,30]. In ramp type flow, under the assumption of chemical equilibrium, it was found that in dissociated air a smaller separation region tends to form because of weaker shock waves. In addition, the heat transfer rates are lower because of lower temperature (dissociation extract thermal energy from the flow). In the case of an impinging-reflecting shock and with consideration of non equilibrium chemistry for air, it is found that the interaction is weakly affected by real gas effects at low Reynolds number. Then, the flow can be computed with a fair degree of accuracy by assuming a constant local value of γ.This assumption may be invalid if the reflection becomes singular (Mach phenomenon). Then an accurate calculation of the adjacent inviscid flow is mandatory. On the hand, at high Reynolds number, chemistry effects lead to substantial differences in the wall pressure and heat transfer distributions, with an increase of the heat transfer levels.

In order to elucidate the incidence of real gas effects on SWBLI experiments were made at Mach numbers ranging from 7.5 to 9.1 in a shock tunnel on a wedge type model with air as working gas [31]. Three stagnation enthalpy levels were considered allowing to achieve un-dissociated, moderately dissociated and highly dissociated cases (in all cases nitrogen dissociation was negligible). The results showed that the scaled upstream interaction length L_u / δ_0 for the three enthalpy levels correlated well with the perfect gas data from other experiments. The same conclusion applied to the pressure plateau coefficient. These results tend to show that in spite of the flow enthalpies being sufficient for chemical reactions, the real gas effects were negligible for the considered test conditions and model size. An interpretation is that the chemical length scale is then much larger than the boundary layer thickness, thus the flow is frozen and there is no influence of relaxation on the interaction. Larger models exposed to flow with higher enthalpies are required to investigate the possible effects of real gas behaviour on SWBLI. Other experiments executed in a larger facility on bigger models were also unsuccessful to exhibit real gas effects on interacting and separated flows, such as base flows [32].

However, major differences between the non catalytic and catalytic wall conditions can be anticipated. In the later case the interaction is much affected by the high energy release in the separated region This induces a dilatation of the separation bubble, like on a heated surface, and a spectacular increase of the wall heat transfer.

2.8 Entropy layer effect

Most hypersonic vehicles have leading edges in order to reduce the heat transfer rate in stagnation regions. Then a detached shock forms in front of the obstacle producing a region of high entropy rise which then surrounds the vehicle surface. This so-called entropy layer is an inviscid fluid feature which takes a special importance in high Mach number flows because of the rapid variation of the shock angle in the detachment region and of the large entropy production through strong shock waves.

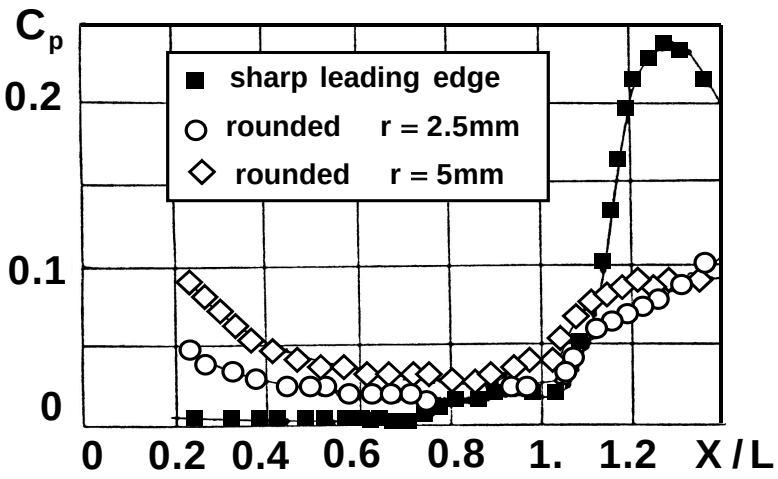

a – wall pressure distribution

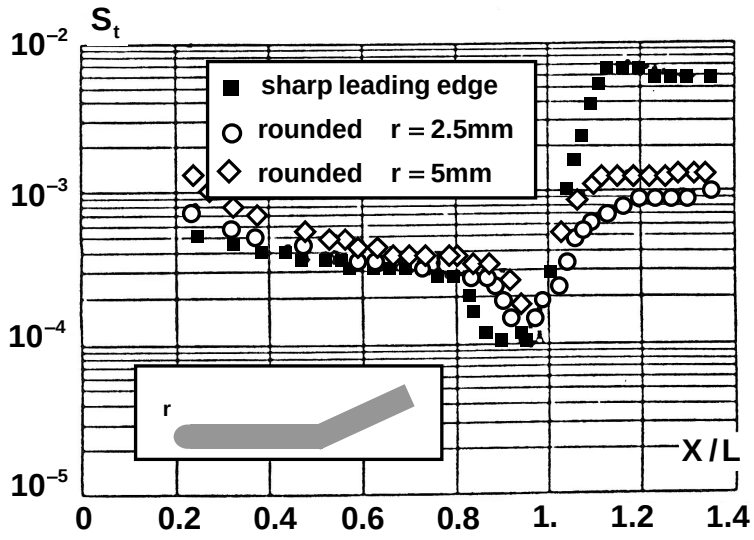

a – wall heat transfer distribution

Figure 20. Entropy layer effect on a ramp induced interaction at Mach 10 [33]

Because of this entropy layer, SWBLI dramatically depend of the leading edge radius of curvature of the plate supporting the ramp model, as shown by the wall pressure and Stanton number distributions plotted in Figure 20,. In these experiments performed at Mach 10, the stagnation conditions were such that the boundary layer was laminar at the interaction onset.

The wall pressure distribution is dramatically affected by blunting of the leading edge: the pressure coefficient on the upstream part of the plate is increased, as a consequence of the Mach number decrease and the pressure level on the ramp is considerably reduced. With the blunt leading edge there is a reduction by a factor of 10 of the peak heat transfer at reattachment. There is also a contraction of the separated zone whose origin, denoted by a decreases in heat transfer, moves in the downstream direction when the leading edge is rounded. This entropy layer effect being due to the stagnation pressure loss through the detached shock ahead of the leading edge, there results a drop in the local Reynolds number and consequently a greater resistance of the flow to separation, in agreement with the free interaction theory (see Section 2.4).

This drop compensates the opposite effect of the local Mach number reduction. In addition, the Reynolds number lowering contributes to maintain a laminar regime throughout the interaction domain, whereas the interaction is transitional when the leading edge is sharp. The combined effects of leading edge bluntness and real gas effect was experimentally studied in a shock tunnel. A considerable reduction in the pressure and heat transfer levels on the ramp where observed when the leading edge is blunted, the separation extent being much smaller. Differences between sharp and blunt leading edge was less pronounced at high enthalpy; this could be due to the reduced stand off distance as a result of dissociation [34].

2.9 Transitional shock wave/boundary layer interactions

As pointed out in the introduction, entirely laminar SWBLI are likely to be encountered at high altitude. With the decrease of altitude during re-entry, there is a rise in Reynolds number so that transition which first occurred far downstream penetrates in the SWBLI region. The effect of laminar-turbulent transition on hypersonic SWBLI is a delicate question which has not yet been completely elucidated, even though experimental evidences allow to characterised the effect [35, 36]. Starting from a fully laminar interaction, it is established that a rise in the Reynolds number R_L provokes a move of transition in the upstream direction until it reaches the reattachment region. Then the peak heat transfer becomes much higher than that of a fully laminar interaction. At the same time, a reversal in the Reynolds number dependence occurs with the separation extent decreasing with an increase of R_L. When R_L is raised, transition first stays in the reattachment region until a limit value of is reached beyond which transition suddenly moves to the separation region. With a further increase of the Reynolds number, transition takes place upstream of the interaction, strongly affecting the flow structure. For instance, the separated zone disappears since the ramp angle (or impinging shock strength) is no longer sufficient to separate the boundary layer. During the transitional phase of the interaction the peak heat transfer at reattachment can be higher than in the fully turbulent case. Such an over-shoot is also observed during boundary layer transition over a flat plate. It can be due to the existence of large and well organised structures, denoting a pre-turbulence state and enhancing transfer mechanisms. Such structures then are broken in smaller eddys once the turbulent regime is established.

Most of the so called ”laminar” hypersonic interactions are in fact transitional since maintaining a laminar regime throughout the interaction domain is difficult due to the extreme sensitivity of the separated shear layer to disturbances. This transition produces a mixed interaction in which separation has the features of a laminar flow (decrease of the heat transfer), whereas reattachment has a turbulent behaviour (higher pressure and heat transfer peaks). This point is a major issue in providing really laminar cases for the validation of computer codes.

3. Problems raised by interaction prediction

Here we shall consider solutions obtained by solving the time averaged Navier-Stokes equation (RANS approach) and do not intend to thoroughly discuss the question of hypersonic flow computations, which would require long developments. We will restrict ourselves to some hard points encountered when computing strongly interacting flows at high Mach number.

3.1 Code numerical accuracy

Interacting flows contain regions of steep gradients either of the wave types (shock, expansion waves) or of the slip line and boundary layer types (shear layers being included) through which the flow properties vary over an extremely short distance. This problem is acute in hypersonic flows where strong shocks interfere to produce wave patterns in which thin shear layer develop along slip lines. Thus the numerical scheme must be enough robust to withstand these rapid flow variations while preserving good accuracy. In addition, these discontinuities, or regions of high gradients, have locations not known in advance which makes their correct capture delicate because of the difficulty to adequately define the computational mesh. The use of schemes based on upwind techniques has in great part solved the problem of the capture of strong discontinuities. Also, adaptive grids offer the possibility to track the regions of high gradients by properly adjusting the refinements of the grid. Nevertheless, application of the most modern codes to strong interactions containing separated regions may lead to large discrepancies with experiments even in the simplest case of laminar flows of a calorically perfect fluid (see [37] for an instructive co-operative action aiming at validating the numerical accuracy of Navier-Stokes and DSMC codes).

3.2 The physical models

Hypersonic SWBLIs raise many difficulties pertaining to the physical modelling itself.

1. Hypersonic interacting flows are the seat of extremely large density variations, especially when there is separation, so that even at relatively high pressure, the continuum regime may be questionable in some parts. Then an hybrid prediction scheme combining the Navier-Stokes equations in the high density regions and DSMC in low density regions may be necessary to adequately model the field [38].
2. The correct prediction of the flow thermodynamics properties requires adequate descriptions of the gas physical and chemical behaviours. This point raises difficult questions, the kinetic of certain non-equilibrium reactions being ill known.
3. The gas transfer properties must be known accurately to correctly predict the skin friction coefficient and the wall heat transfer (vital for a proper sizing of the thermal protections).
4. In a reacting gas, wall heat transfer depends on the chemical state at the wall (species concentration). For non-equilibrium flows, catalytic effects have a dramatic influence, heat transfer being minimised on a non catalytic wall, or amplified on a fully catalytic wall. As indicated in Section 2.7, the energy release occurring when the wall is catalytic greatly affects the size of a separated region acting like a strong heating of the surface.
5. Laminar-turbulent transition has a dramatic influence on SWBLI. The difference between laminar and turbulent interactions has been emphasised and is well known. However, transition may have a more subtle influence when it takes place in the interaction

itself at it is frequent in hypersonic flows. Prediction of transition in such a complex situation is a challenge only recently addressed [36, 39, 40].

6. The most challenging problem met in the prediction of hypersonic SWBLIs is the modelling of turbulence. Much work has been devoted to this question with modest success. Usual transport equations models perform relatively well in the prediction of interacting flows, provided that the Mach number be not too high and the separated zone, if it exists, small. The situation is not so satisfactory in shock separated flows with extended separation and up to now, none of the proposed models gives really satisfactory results. Turbulence behaviour in this kind of flow is dictated by the conjugated action of several factors :

- At Mach number above 6, terms involving density fluctuations in the time-averaged equations, the so-called compressibility terms, become significant and can no longer be neglected.
- As seen above, in hypersonic SWBLIs the shocks penetrate into the boundary layer leading to shock/turbulence interaction which may have important consequences on the turbulence further development.
- Flow unsteadiness may cause an amplification of turbulence by promoting momentum exchange between the outer stream and the boundary layer [41].
- A key factor probably more important than the previous ones is the existence of a separated region containing a shear layer along which turbulent structures undergo rapid growth. At separation, there is a change in the turbulence scale from a scale which is of the order of the boundary layer thickness to a free shear layer type scale which grows in proportion to the shear layer development length. At reattachment, the reverse process takes place. Such changes in scales are difficult to model by the classical RANS approach [42]
- In extreme conditions there is a coupling between turbulence and chemistry activity of the flow through ill known mechanisms [43].
- Prediction of 3D interactions, which are the most likely to occur in real conditions, not only necessitates representative turbulence models but also high numerical accuracy [44].

The greatest discrepancies between experiment and theory are noticed in the prediction of the peak heat transfer at reattachment. Thorough examinations of the question have shown that discrepancy cannot be attributed to compressibility terms [45]. The classical RANS approach is certainly to be reconsidered, but it is also clear that bad prediction could be due to insufficient numerical accuracy.

4. Conclusion

Shock wave/boundary layer interactions in hypersonic flows are characterised by extremely large pressure variations and intense thermal effects, especially when the shock is strong enough to separate the boundary layer. Due to their repercussions on the vehicle performance (stability) and on the thermal loads, SWBLIs are of major concern for designers who would appreciate to have at their disposal more reliable predictive tools. Strong interactions have been extensively studied in the past, both from the experimental and theoretical point of view. Thus, the physics of SWBLI can be considered as well understood, at least for 2D flows (planar and axisymmetric). Analyses like the free interaction theory, conforted by a wealth of experimental evidences, have permitted to elucidate and quantify the influence of parameters

such as the configuration geometry (ramp flows, incident-reflecting shock, adaptation shock), the Mach number, the Reynolds number, the wall temperature. Correlation laws are available to predict, with a limited accuracy, the conditions for shock-induced separation, the heat transfer peaks in an interaction, the upstream influence length. However, in spite of spectacular progress over the past 30 years, the predictive capabilities are still limited because of the numerical and modelling difficulties met in hypersonic interacting flow calculations when the boundary layer is turbulent. From the physical point of view, SWBLIs in truly hypersonic flows imply complex phenomena which are not yet fully understood or even identified. There is not a clear assessment of the specific influence of real-gas effects on interacting flows, although this point is probably not the most crucial. Decisive progress in this domain requires carefully made experiments in hypersonic facilities with the use of sophisticated optical methods to perform field measurements providing information on the flow properties and gas composition. Laminar to turbulent transition has dramatic influence on interacting flows, especially when it occurs in the interaction region itself or its immediate vicinity. In spite of its importance this point has been scarcely studied and it is only recently that an in depth examination of transitional SWBLIs has been undertaken. This subject would merit a more intense research effort both from the experimental and theoretical sides. In particular, it would be instructive to elucidate and quantify more precisely the influence of wall temperature on transitional interactions.

Turbulence modelling in high Mach number SWBLIs is a huge and still largely open problem. The usual transport equation models perform poorly as soon as a separated region forms. Turbulence in interacting flows involve many aspects: compressibility, shock/turbulence interactions, rapid compression effects, flow unsteadiness, turbulence/chemistry coupling, transfer mechanisms, to name the most important. Calculation of 3D interactions is also a formidable challenge since in addition one has to consider the complex topology of three-dimensional flows and specific phenomena such as vortex formation, shock/vortex interaction and vortex breakdown. It is clear that decisive advances in this domain will require a considerable effort to obtain both detailed and reliable experimental data and to develop more realistic physical models.

5. References

[1] Délery, J. and Marvin, J.G.: *Shock wave/Boundary Layer Interactions.* AGARDograph N° 280, 1986

[2] Holden, M. : A review of aerothermal problems associated with hypersonic flights. *AIAA Paper 77-0045*, 1986

[3] Settles, G.S: Swept shock/boundary layer interaction scaling laws, flow field structure and experimental methods. *AGARD/FDP VKI Special Course on Shock Wave/Boundary Layer Interactions in Supersonic and Hypersonic Flows, AGARD Report N° 792*, 1993

[4] Délery, J. Shock interaction phenomena in hypersonic flows. Part II: Physical features of shock wave/boundary layer interaction in hypersonic flows. *AGARD Conference on Future Aerospace Technology in the Service of the Alliance*, 144-16 April 1997, Ecole Polytechnique, Palaiseau (France)

[5] Edney, B: Anomalous heat transfer and pressure distributions on blunt bodies at hypersonic speeds in the presence of an impinging shock. Aeronautical Research Institute of Sweden, FFA Report 115, Stockholm, 1968

[6] Délery, J. and Panaras, A.G.: Shock wave/boundary layer interactions in high Mach number flows. *AGARD/FDP WG 18 on Hypersonic Experimental and Computational Capability, Improvement and Validation, AGARD AR 319, Vol. I*, 1996

[7] Panaras, A.G.: Review of the physics of swept-shock/boundary layer interactions. *Prog. Aerospace Sci.,* Vol. 32, pp.173-244, 1996
[8] Zheltovodov, A.A.: Shock wave/turbulent boundary layer interactions. Fundamental studies and applications. *AIAA Paper 96-1977*, 1996
[9] Délery, J.: Basic experiments on high Mach number two-dimensional and three-dimensional separated flows. *Experimentation, Modeling and Computation in Flow, Turbulence and Combustion,* Vol.1, Ed. J.A. Désidéri, B.N. Chetverushkin, Y.A. Kuznetsov, J. Périaux and B. Stoufflet, Wiley, 1996
[10] Shang, J.S., Hankey, W.L. Jr. And Law, C.H.: Numerical simulation of shock wave/turbulent boundary layer interaction. *AIAA Journal,* Vol. 14, N°10, Oct. 1976, pp. 1451-1457, 1976
[11] Lighthill, M.J.: On boundary layer upstream influence. Part II : Supersonic flows without separation. *Proc. Roy. Soc.,* **A (217),** pp. 478-507, 1953
[12] Stewartson, K. and Williams, P.G.: Self-induced separation. *Proc. Roy. Soc.,* **A (312),** pp. 181-206, 1969
[13] Settles, G.S.: An experimental study of compressible boundary layer separation at high Reynolds number. *Ph. D. Thesis, Princeton University,* 1975
[14] Délery, J. : Shock phenomena in high speed aerodynamics: still a source of major concern. *The Aeronautical Journal of the Royal Aeronautical Society* , Jan. 1999
[15] Elfstrom, G.M. Turbulent hypersonic flow at a wedge compression corner. *J. Fluid Mech.,* Vol. 53, Part 1, pp. 113-129, 1972
[16] Chanetz, B.: ONERA hypersonic test-cases in the framework of the Working Group 18. *AGARD/FDP WG 18 on Hypersonic Experimental and Computational Capability, Improvement and Validation, AGARD AR 319, Vol. II*, 1997
[17] Holden, M.: Shock wave/turbulent boundary layer interactions in hypersonic flows. *AIAA Paper 72-0074*, 1972
[18] Chapman, D.R., Kuhen, D.M. and Larson, H.K.: Investigation of separated flows in supersonic and subsonic streams with emphasis on the effect of transition. *NACA TN-3869,* 1957
[19] Zhukoski, E.E.: Turbulent boundary layer separation in front of a forward-facing step. *AIAA Journal,* Vol. 5, N° 10, Oct. 1967, pp. 1746-1753, 1967
[20] Roshko, A. and Thomke, G.J.: Flare-induced interaction lengths in supersonic, turbulent boundary layers. *McDonnell DouglasMDAC Paper WD 2416.* Also : *AIAA Journal,* Vol. 14, N° 7, July 1974, pp. 873-879, 1974
[21] Lewis, J.E., Kutoba, T. and Lees, L.: Experimental investigation of supersonic laminar two-dimensional boundary layer separation in a compression corner with and without cooling. *AIAA Paper 67-0191*. Also : *AIAA Journal,* Vol. 6, N°1, Jan. 1967, pp. 7-14, 1967
[22] Spaid, F.W. and Frishett, J.C.: Incipient separation of a supersonic, turbulent boundary layer, including effects of heat transfer. *AIAA Journal,* Vol. 10, N°7, July 1972, pp. 915-922, 1972
[23] Gautier, B.: Etude théorique et expérimentale des effets du refroidissement pariétal sur l'interaction onde de choc – couche limite laminaire en écoulement plan hypersonique (Theoretical and experimental study of wall cooling effect on laminar shock wave/boundary layer interaction in planar hypersonic flow*). Ph. D. Thesis, Université Libre de Bruxelles*, 1972
[24] Délery, J.: Etude expérimentale de la réflexion d'une onde de choc sur une paroi chauffée en présence d'une couche limite turbulente (Experimental investigation of the reflection of a

shock wave on a heated surface in presence of a turbulent boundary layer). *La recherche Aérospatiale, N°1992-1, Jan.-Feb. 1992, pp. 1-23 (French and English editions),* 1992
[25] Curle, N.: The effects of heat transfer on laminar boundary layer separation in supersonic flow. *Aero. Quart*., Vol. 12, pp. 309-336, 1961
[26] Délery, J. and Chanetz, B.: Experimental aspects of code verification/validation: Applications to internal aerodynamics, *VKI-Lecture Series 2000-08: Verification and Validation of Computational Fluid Dynamics*, June 5-8, 2000
[27] Délery, J. and Coët, M.-C.: Experiments on shock wave/boundary layer interactions produced by two-dimensional ramps and three-dimensional obstacles. *Workshop on Hypersonic Flows for Re-entry Problems,* Antibes, France, 1990
[28] Hung, F.T. and Barnett, D.O.: Shock wave/boundary layer interference heating analysis. *AIAA Paper 72-0237*, 1973
[29] Grasso, F. and Leone, G.: Chemistry effects in shock wave/boundary layer interaction problems. IUTAM *Symposium on Aerothermochemistry of Spacecraft and Associated Hypersonic Flows,* Marseille, France, 1992
[30] Grummet, A.A., Anderson, J.D. and Lewis, M.J.: A numerical study of shock wave/boundary layer interaction in non-equilibrium chemically reacting air. The effects of catalytic walls. *AIAA Paper 91-0245*, 1991
[31] Mallinson, S.G., Gai, S.L. and Mudford, N.R.: High enthalpy, hypersonic compression corner flow. *AIAA Journal,* Vol. 34, N°6, June. 1996, pp. 1130-1137, 1996
[32] Holden, M., Bergman, R., Harvey, J., Boyd, I. and George, J.: Experimental studies of real-gas effects over a blunted cone/flare configuration in hypervelocity flows. *AIAA Paper 97-0855*, 1997
[33] Coët, M.-C., Délery, J. and Chanetz, B.: Experimental study of shock wave/boundary layer interaction at high Mach number with entropy layer effect. *IUTAM Symposium on Aerothermochemistry of Spacecraft and Associated Hypersonic Flows,* Marseille, France 1992
[34] Don Gray, J. and Rhudy, R.W.: Effects of blunting and cooling on separation of laminar supersonic flow. *AIAA Journal,* Vol. 11, N°19, Sept. 1973, pp. 1296-1301, 1973
[35] Heffner, K.: Contribution à l'étude d'une rampe de compression en écoulement hypersonique. Partie I : Régime de transition laminaire-turbulent de la couche limite. Partie II : Régime de transition écoulement continu - écoulement moléculaire libre (Contribution to the study of a compression ramp in hypersonic flow. Part I : Laminar to turbulent transition regime of the boundary layer. Part II : Transition from free molecular to continuum regime). *Ph. D. Thesis, University Pierre et Marie Curie, Paris*, 1993
[36] Vandomme, L., Chanetz, B., Benay, R. and Perraud, J.: Transitional shock wave/boundary layer interactions in hypersonic flow at Mach 5. *12th AIAA International Space Planes ans Hypersonic Systems and Technologies*, Norfolk, 15-19 December 2003
[37] Chanetz, B., Benay, R., Bousquet, J.-M., Bur, R., Pot, T., Grasso, F. and Moss, J.: Experimental and numerical study of the laminar separation in hypersonic flow. *Aerospace Science and Technology*, N°3, pp-205-218, 1998
[38] Holden, M., Harvey, J., Boyd, I., George, J. and Horvath, T.: Experimental and computational studies of the flow over a sting mounted planetary probe configuration. *AIAA Paper 97-0768*, 1997
[39] Arnal, D.: Boundary layer transition prediction based on linear theory. *AGARD/FDP-VKI Special Course on Progress in Transition Modeling, AGARD Report 793*, 1994

[40] Grasso, F., Leone, D. and Délery, J.: Validation procedure for the analysis of shock wave/boundary layer interaction problems. *AIAA Journal,* Vol. 32, N°9, Sept. 1994, pp. 1820-1827, 1994
[41] Dolling, D.S.: Unsteady phenomena in shock wave/boundary layer interaction. *AGARD/FDP-VKI Special Course on Shock Wave/Boundary Layer Interactions in Supersonic and Hypersonic Flows, AGARD Report N°792*, 1993
[42] Grasso, F. and Falconi D.: High-speed turbulence modeling of shock wave/boundary layer interaction. *AIAA Journal,* Vol. 31, N°7, July 1993, pp. 1199-1206, 1993
[43] Leclère F. and Aupoix, B.: Hypersonic turbulent nonequilibrium reactive nozzle flow calculations. *ICAS 94, 19th Congress of the International Council of the Aeronautical Sciences,* Anaheim, California, 18-23 Sept. 1994
[44] Knight, D.D.: Numerical simulation of 3-D shock wave/turbulent boundary layer. *AGARD/FDP VKI Special Course on Shock Wave/Boundary Layer Interactions in Supersonic and Hypersonic Flows, AGARD Report N° 792,* 1993
[45] Douay, G.: Modélisation et étude numérique de la turbulence compressible en écoulement supersonique (Modeling and numerical study of compressible turbulence in supersonic flow). *Ph. D. Thesis, University of Rouen, France*, 1994